This is a non-peer reviewed preprint submitted to EarthArXiv.

Mapping Europe's Natural Hydrogen Potential: A Continental-Scale Geological Prospectivity Assessment

Florian H. J. Willemsen[1], Johannes M. Miocic[1*]

[1]GeoEnergy, Energy and Sustainability Research Institute Groningen, University of Groningen, Nijenborgh 6, 9747 AG Groningen, the Netherlands

[*]Corresponding author: j.m.miocic@rug.nl

Abstract

Natural hydrogen, generated by a range of geological processes in the Earth's crust, is emerging as a promising carbon-neutral energy source. However, systematic large-scale assessments of its subsurface occurrence remain limited. This study presents the first continental-scale prospectivity map of natural hydrogen in Europe, integrating geological indicators of hydrogen generation, reservoir quality, and sealing capacity. A comprehensive inventory of ultramafic rock bodies—key indicators of hydrogen potential—is compiled and spatially analysed. To address geological uncertainty, we apply Monte Carlo simulations, yielding conservative, median, and optimistic resource estimates. High-prospectivity regions are identified in Hungary, Denmark, Poland, and Serbia, with many documented hydrogen occurrences aligning with predicted source zones. This spatial assessment provides a critical framework for early-stage exploration, supports future energy security strategies, and highlights key regions for focused research and development in the context of the energy transition.

Keywords: Natural hydrogen; Prospectivity mapping; Serpentinization; Radiolysis; Ultramafic rocks; Geological exploration; Monte Carlo simulation; Energy transition; Europe

1. Introduction

The global transition to carbon-neutral, renewable-based energy systems is essential to mitigate the effects of climate change and limit global warming (Rogelj et al., 2015). The configuration of regional decarbonized energy systems depends not only on the spatial distribution and availability of renewable energy sources but also on demand profiles, infrastructure interconnectivity, and the suitability of specific energy carriers for various applications. Among these carriers, hydrogen has received growing attention due to its versatility in sectors such as transportation, industry, and energy storage (Hanley et al., 2018; McPherson et al., 2018). Despite this potential, over 95% of hydrogen currently in use is derived from fossil fuels, leading to considerable carbon dioxide emissions (IRENA, 2023). Key barriers to scaling up low-carbon hydrogen include the high cost of green hydrogen production and the competitiveness of other renewable-based technologies for many applications (Liebreich et al., 2023).

In this context, natural hydrogen—also known as *white* or *gold hydrogen*—is emerging as a promising, potentially low-cost and low-emission alternative. Generated by geological processes such as serpentinization, radiolysis, and iron oxidation within the Earth's crust, natural hydrogen has long been observed at surface seeps, particularly in tectonic and mid-ocean ridge settings. However, early assessments dismissed the likelihood of significant subsurface accumulations due to the gas's high diffusivity and reactivity (USGS, 1993; Zgonnik et al., 2015).

Renewed interest in the last two decades (Smith et al., 2005; Zgonnik, 2020) has been driven by growing evidence that natural hydrogen may occur more broadly than previously believed. Recent estimates suggest that the subsurface generation of hydrogen may amount to thousands to billions of megatons globally (Ellis & Gelman, 2024). However, the economic viability of these resources remains uncertain, depending heavily on depth, geological setting, and the physical state of the hydrogen—whether free gas or dissolved in formation waters. Cost estimates vary widely: some studies suggest that natural hydrogen could be more affordable than both green and grey hydrogen (Rigollet & Prinzhofer, 2022), while others express scepticism regarding scalability and accessibility (Patonia et al., 2024). Similarly, the question whether natural H_2 could be considered renewable is disputed, with some indicating that it may not be (Brunet & Malvoisin, 2025).

Effective exploration is therefore essential to assess the distribution and extractability of natural hydrogen. Existing detection methods, such as soil gas sampling, are spatially limited and often ambiguous in distinguishing active hydrogen seeps from background signals (Lévy et al., 2023; Aimar et al., 2023). In response, geologically based prospectivity assessments have been proposed to prioritize areas for more detailed investigation. One such effort is the recent prospectivity mapping of the United States by Gelman et al. (2023), which incorporated indicators of hydrogen sources, reservoirs, and seals.

In this study, we apply a similar methodology to construct the first continent-wide natural hydrogen prospectivity map for Europe. We integrate multiple geological datasets, including a comprehensive inventory of ultramafic complexes and updated records of hydrogen occurrences—some previously undocumented. Unlike earlier regional studies (e.g., Donzé et al., 2024; Gaucher et al., 2023), our work offers a systematic assessment of hydrogen generation potential at the continental scale. By addressing geological uncertainty through Monte Carlo simulations, we provide conservative, median, and optimistic resource estimates. This work aims to support the strategic exploration of natural hydrogen resources in Europe and to contribute to the continent's broader goals of energy transition and resilience.

2. Methodology

To identify regions with high natural hydrogen prospectivity, geological indicators related to hydrogen sources, reservoirs, and seals were integrated using GIS software (QGIS). The selected indicators are listed in Table 1, and their presence was determined based on publicly available geological datasets (e.g., EGDI, IGME) and relevant literature. Following the methodology developed by Gelman et al. (2025), each indicator was assigned a chance of sufficiency (COS) value. The COS represents the fractional probability that a given feature is both present and effective in contributing to hydrogen accumulation. These values were established by a panel of experts, and where indicators overlap with those used in Gelman et al. (2025), the same COS values and spatial buffers were adopted. This approach results in a relative prospectivity score—not a statistical probability—that allows for comparison across regions at a continental scale. It is particularly suited to early-stage exploration where data constraints preclude precise quantification. Details of the calculation procedures for composite layers are provided in Supplementary Material C.2.

To account for geological uncertainty, Monte Carlo simulations (n = 1,000) were performed by sampling COS values from triangular probability distributions defined by low, median (mode), and high estimates for each indicator (Table 1). This yields P10, P50, and P90 maps representing optimistic, median, and conservative prospectivity scenarios, respectively. P50 maps are presented in the main text, while P10 and P90 maps are included in Supplementary Materia B.

Table 1 | *Geological indicators included in the prospectivity analysis, and chance of sufficiency (COS) values for each layer, used in the uncertainty analysis (triangular distribution Monte Carlo simulation). *Buffer is given a larger radius based on the size of the uranium deposit, see Supplementary Material C.1.*

Layer	COS low	COS med	COS high	Spatial buffer
Serpentinization (SER)				
SER1 - Ultramafic rocks (-)	0.5	0.6	0.7	20 km
SER2 - Ultramafic rocks (o)	0.6	0.7	0.8	20 km
SER3 - Ultramafic rocks (+)	0.7	0.8	0.9	20 km
SER4 - Isostatic gravity	0.1	0.4	0.7	-
SER5 - Failed rifts	0.7	0.8	0.9	-
SER6 - Rift-inversion orogens	0.7	0.8	0.9	-
SER7 - Banded iron formations	0.6	0.7	0.8	20 km
SER8 - Every other area	0	0.1	0.2	-
Radiolysis (RAD)				
RAD1 – Uranium occurrence	0.1	0.2	0.3	Varies*
RAD2 - Precambrian craton	0.5	0.7	0.9	100 km
RAD3 - Accreted terranes	0.1	0.2	0.5	100 km
Deep source (DEE)				
DEE1 - Faults	0.1	0.2	0.3	10 km
DEE2 - Suture zones	0.2	0.5	0.8	40 km
DEE3 - High heat flow	0.5	0.7	0.9	-
DEE4 - Heat flow buffer	0.1	0.2	0.3	-

DEE5 - Every other area	0	0.1	0.2	-
Reservoir (RES)				
RES1 - Sedimentary rocks	0.8	0.95	1	-
RES2 – Igneous / Metamorphic rocks	0.7	0.8	0.9	-
RES3 - Sedimentary basins	1	1	1	-
Seal (SEA)				
SEA1 - Subsurface salt	0	0.1	0.2	-
SEA2 - Sedimentary rocks	0.6	0.8	1	-
SEA3 – Igneous / Metamorphic rocks	0.2	0.5	0.8	-
SEA4 - Sedimentary basins	0.1	0.3	0.5	-

3. Results

3.1 *Sources of natural hydrogen*

3.1.1 Serpentinisation

Hydrogen can be produced through serpentinization, a geochemical reaction involving the hydration of ultramafic rocks—typically rich in iron and low in silica—by water. As ultramafic rocks are key precursors for this process, their distribution serves as a primary indicator of hydrogen generation potential.

Due to the lack of a comprehensive ultramafic rock dataset for Europe, a compilation of ophiolitic complexes was used as a proxy. Ophiolites—tectonically emplaced fragments of oceanic lithosphere—often contain ultramafic rocks derived from the Earth's upper mantle. However, not all ophiolites contain ultramafic material, and not all ultramafic rocks are ophiolitic in origin (Zuo et al., 2022; Pomonis & Magganas, 2017). Therefore, a systematic literature review was conducted to verify the composition of individual ophiolites and to identify additional, non-phiolitic ultramafic bodies. This included analysis of geomagnetic data, cross-sections, and petrological studies. A complete list of identified ultramafic occurrences is provided in Table A1 (Supplementary Material).

Depth is also a critical factor: serpentinization is most efficient between depths of approximately 4 to 21 km, depending on the geothermal gradient (Zgonnik, 2020; Criss, 2019). Accordingly, each occurrence was classified based on depth constraints and assigned a COS value: high (SER3, '+'), medium (SER2, 'o'), or low (SER1, '–'). Figure 1 shows the mapped ultramafic bodies and ophiolite complexes, labeled according to Table A1. These occurrences are concentrated in orogenic zones such as the Alps.

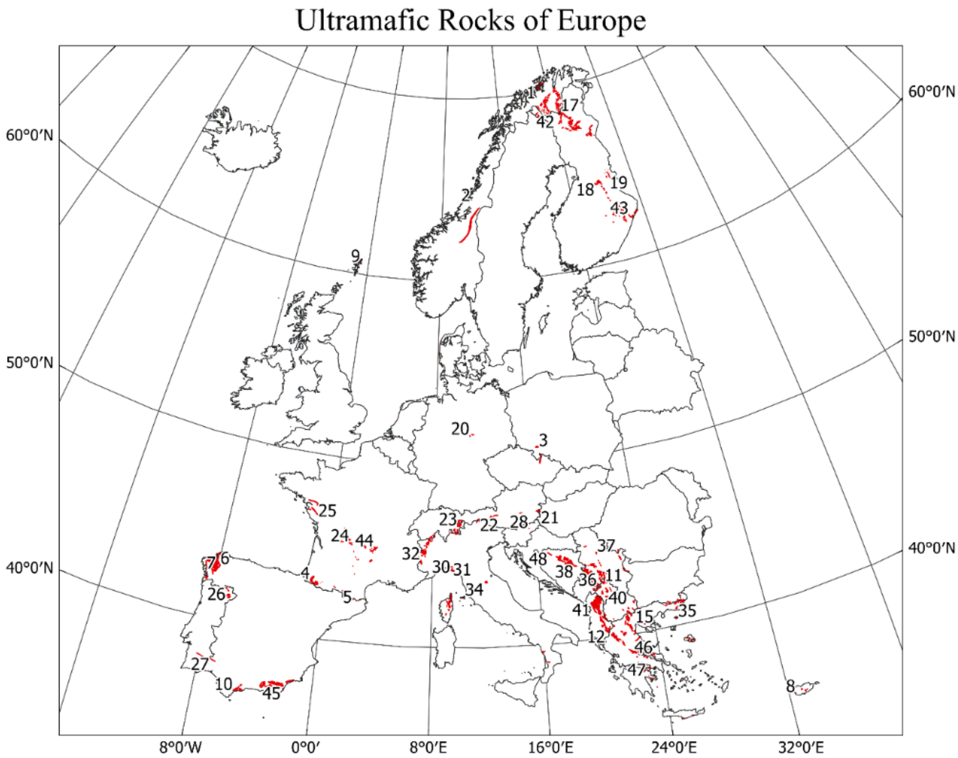

Figure 1 | Distribution of ultramafic bodies and ophiolitic complexes across Europe. Labels correspond to entries in Table A1. Only ophiolites confirmed to contain ultramafic material are included.

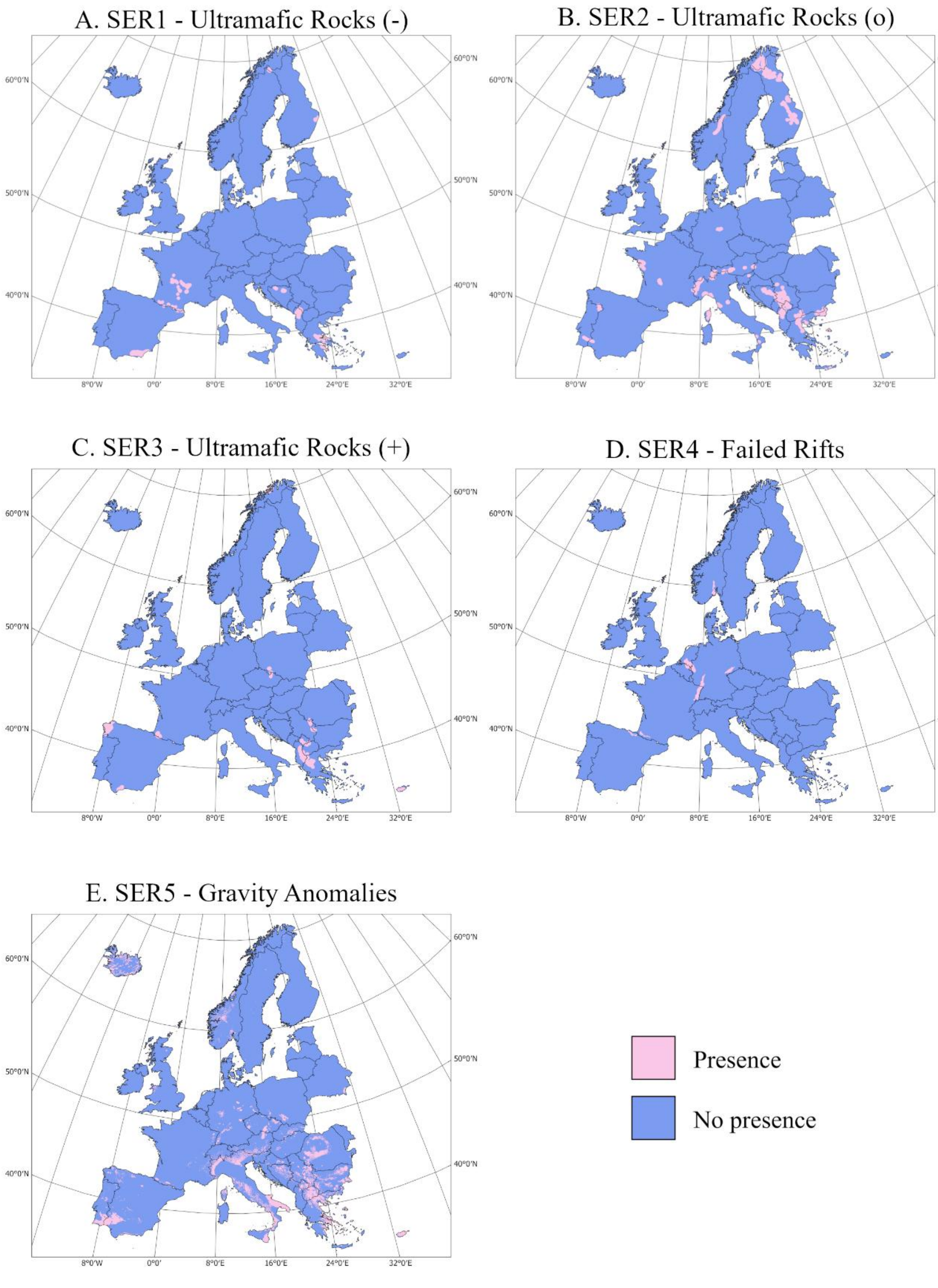
A. SER1 - Ultramafic Rocks (-)
B. SER2 - Ultramafic Rocks (o)
C. SER3 - Ultramafic Rocks (+)
D. SER4 - Failed Rifts
E. SER5 - Gravity Anomalies
Presence
No presence

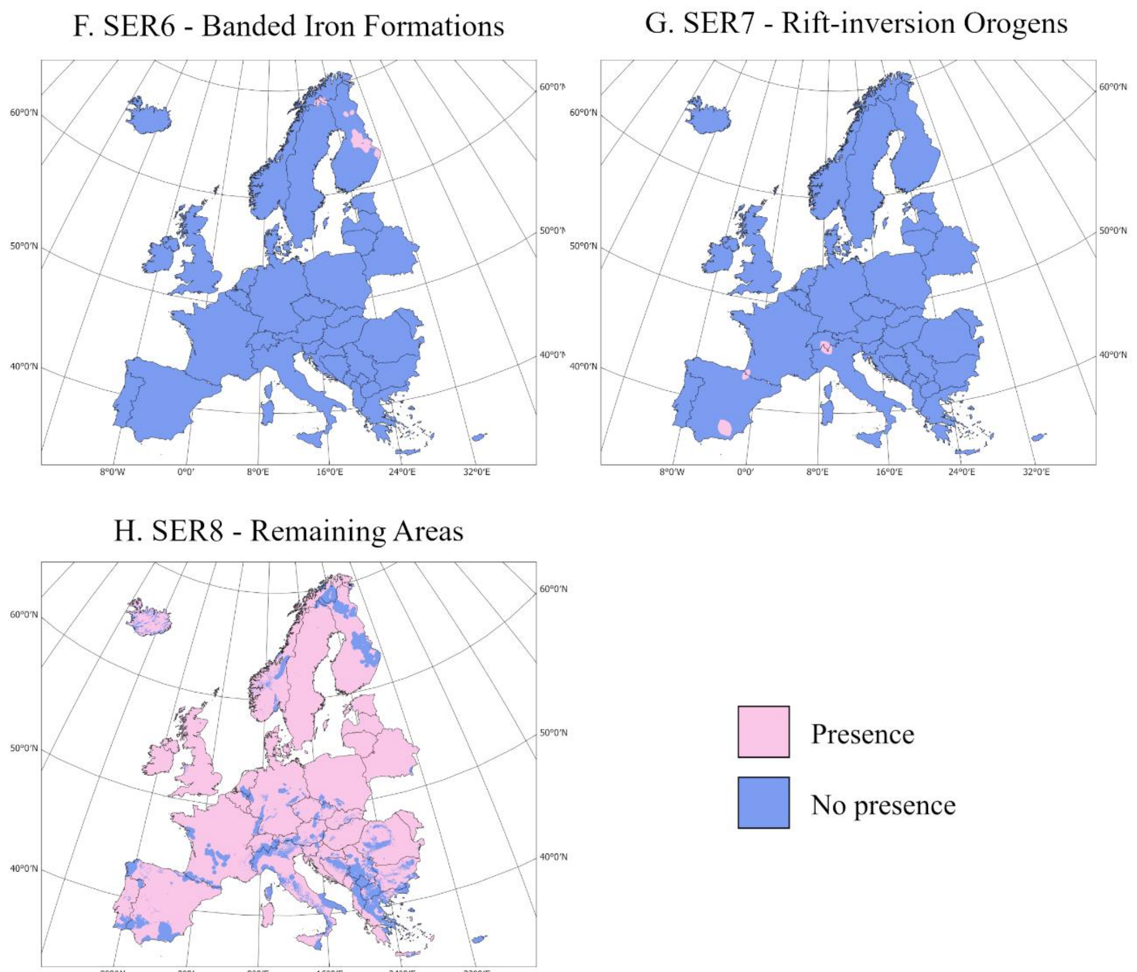

Figure 2 | *Geological indicators included in the serpentinization (SER) source layer.* ***A–C:*** *Ultramafic bodies with low (SER1), medium (SER2), and high (SER3) COS.* ***D****: Failed rift systems (SER4).* ***E****: Gravity anomalies >40 mGal (SER5).* ***F****: Banded iron formations (SER6).* ***G****: Rift-inversion orogens (SER7).* ***H:*** *Remaining areas.*

The serpentinization composite layer comprises eight sublayers (SER1–SER8), as shown in Figure 2. The first three layers (SER1-SER3) reflect the spatial distribution of ultramafic bodies with a 20 km buffer and COS weights based on depth classification. SER4 includes failed rift systems, which can expose mantle rocks via crustal thinning and isostatic uplift (Gillard et al., 2019; Gelman et al., 2025). SER5 represents positive gravity anomalies exceeding 40 mGal, which may indicate dense ultramafic material in the subsurface (Escartin & Cannat, 1999; Bureau Gravimétrique International, 2012). SER6 includes banded iron formations, capable of generating hydrogen through low-temperature oxidation of ferrous iron (Geymond et al., 2022). SER7 identifies rift-inversion orogens—recently proposed as potential hydrogen-rich structures due to mantle exhumation and favorable trapping conditions (Zwaan et al., 2025). SER8 encompasses all other areas not covered by the previous sublayers and is assigned a uniform, low COS value to account for unidentified sources. Figure 3 shows the resulting composite serpentinization source layer, integrating SER1–SER8 using the COS values from Table 1.

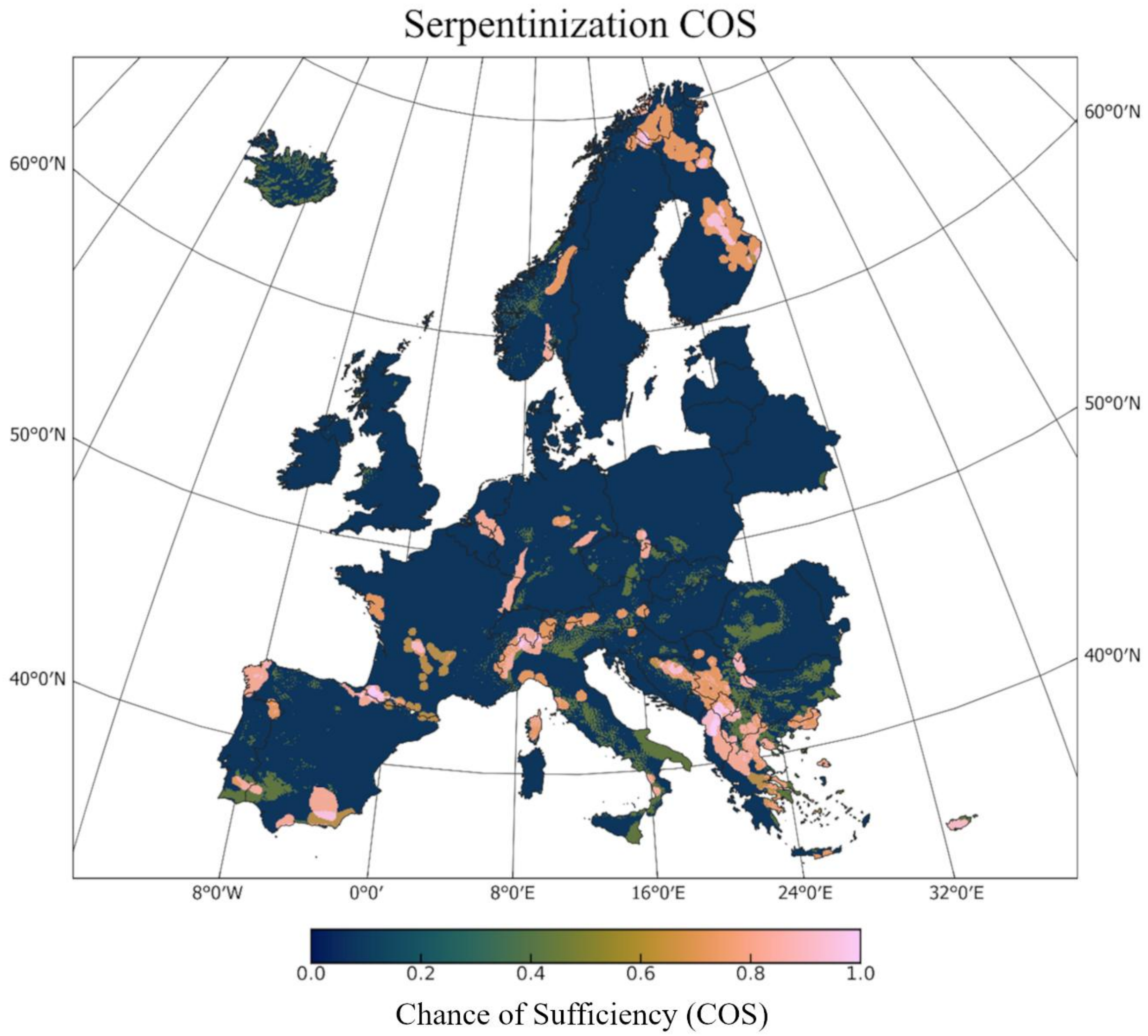

Figure 3 | *Composite COS map for serpentinization sources, based on SER1–SER8.*

3.1.2 Radiolysis

Radiolysis involves the dissociation of water molecules by ionizing radiation, forming reactive species that recombine to produce molecular hydrogen. This process occurs in the presence of radioactive materials such as uranium and thorium. Three geological indicators were included (Figure 4): RAD1: Documented uranium occurrences across Europe, buffered according to deposit size (EGDI, 2021). RAD2: The East European Craton—composed of stable, uranium-enriched Precambrian basement rock (Asch, 2005; Lollar et al., 2014). RAD3: Accreted terranes, representing geologically younger regions with variable radiogenic potential and less time for hydrogen accumulation (Gelman et al., 2025). This layer serves as the inverse of RAD2. Phanerozoic granitoids were excluded due to limited data coverage across Europe and their low expected contribution. Figure 5 presents the composite COS map for radiolysis sources, constructed from RAD1–RAD3 and corresponding COS values from Table 1.

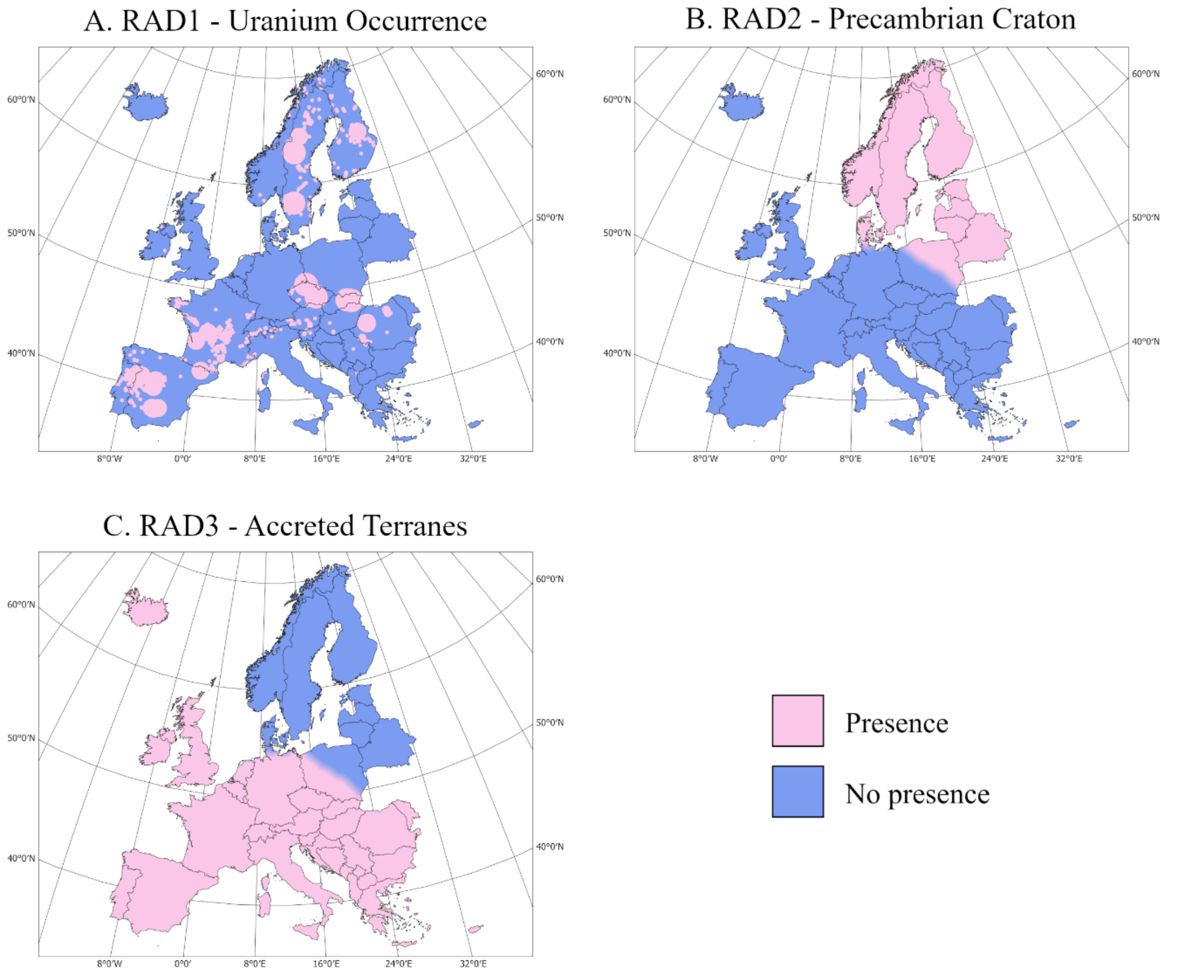

Figure 4 | *Geological indicators for radiolysis (RAD) source layer.* ***A:*** *Uranium occurrences (RAD1).* ***B:*** *East European Craton with 100 km buffer (RAD2).* ***C:*** *Accreted terranes with 100 km buffer (RAD3).*

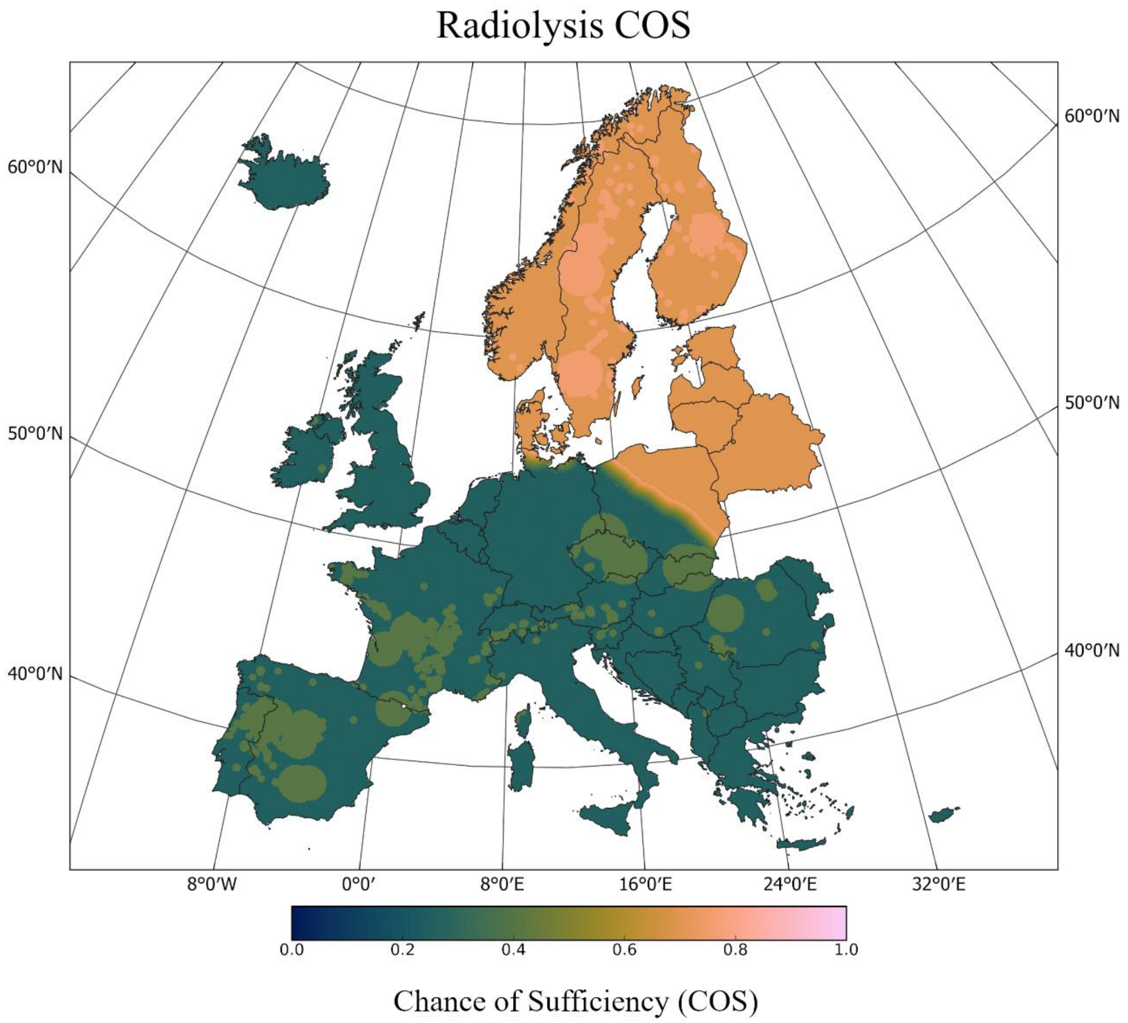

Figure 5 | *Composite COS map for radiolysis sources based on layers RAD1–RAD3.*

A clear spatial differentiation is observed between the East European Craton and the younger, geologically complex regions of central and western Europe. High COS values dominate in Scandinavia and the Baltic states, consistent with extensive, long-lived radiolytic environments.

3.1.3 Deep sources

Hydrogen generated in the Earth's mantle via degassing or deep serpentinization may migrate upward through the crust. The identification of migration pathways and thermal regimes is critical in assessing this deep source potential. The deep source composite layer includes five indicators (Figure 6): DEE1: Major fault systems with a 10 km buffer, representing conduits for upward gas migration (Liu et al., 2023). DEE2: Suture zones—boundaries between tectonic terranes—which are favorable for fluid transport (Lefeuvre et al., 2024). DEE3: Regions of elevated heat flow (>80 mW/m^2), associated with enhanced hydrothermal circulation and gas mobility (Chamorro et al., 2013). DEE4: A transition buffer zone (70–80 mW/m^2), assigned lower COS values. DEE5: Residual areas not covered by the above features, with a minimal COS value assigned to account for unknown sources. The composite deep source layer, shown in Figure 7, reflects increased hydrogen prospectivity in regions with dense fault networks and elevated heat flow, particularly in Iceland and parts of France.

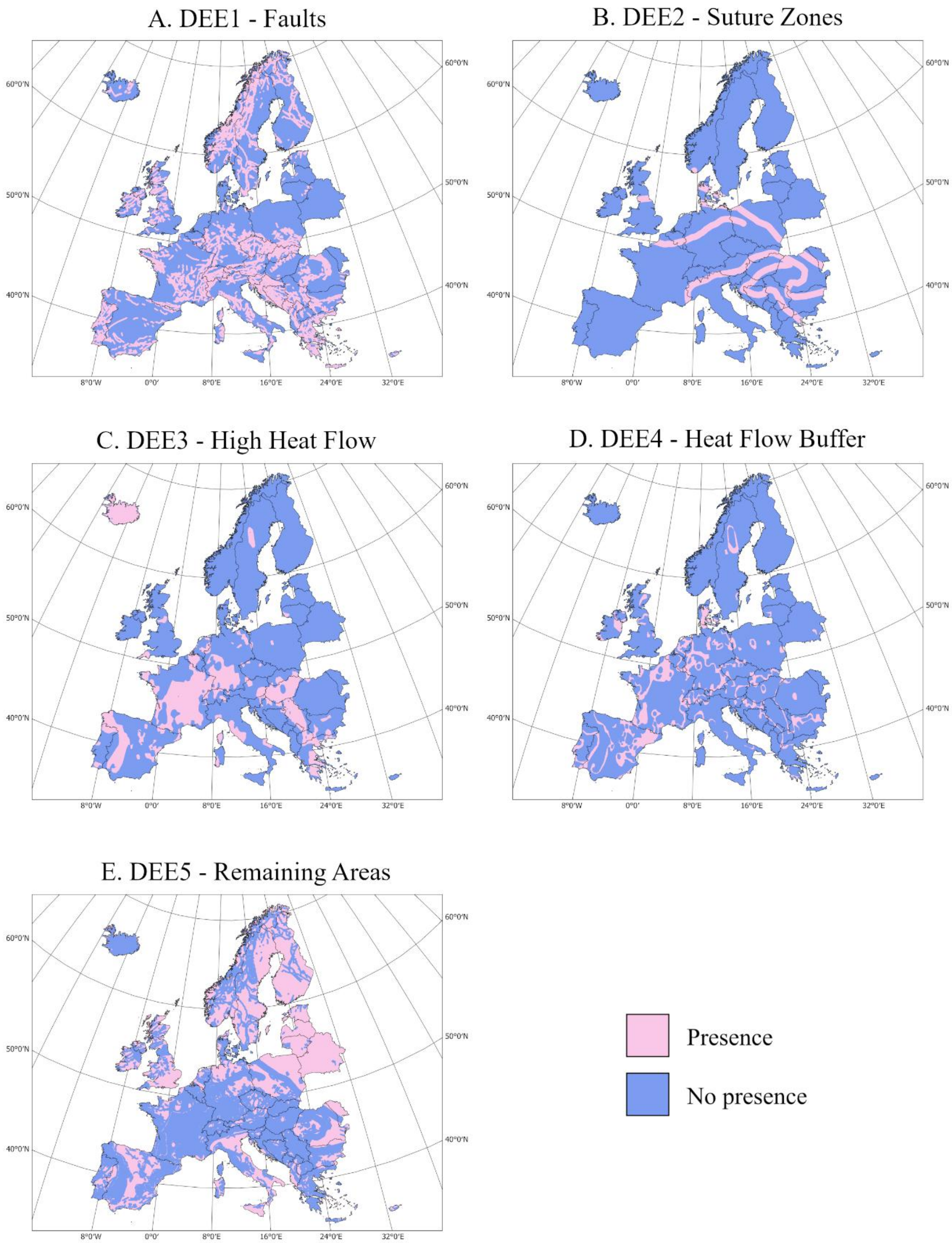

Figure 6 | *Geological indicators for deep source (DEE) potential.* ***A:*** *Faults with 10 km buffer (DEE1).* ***B:*** *Suture zones with 40 km buffer (DEE2).* ***C:*** *Heat flow >80 mW/m*^{2} *(DEE3).* ***D:*** *Transition heat flow zone (70–80 mW/m*^{2}*, DEE4).* ***E:*** *Residual areas (DEE5).*

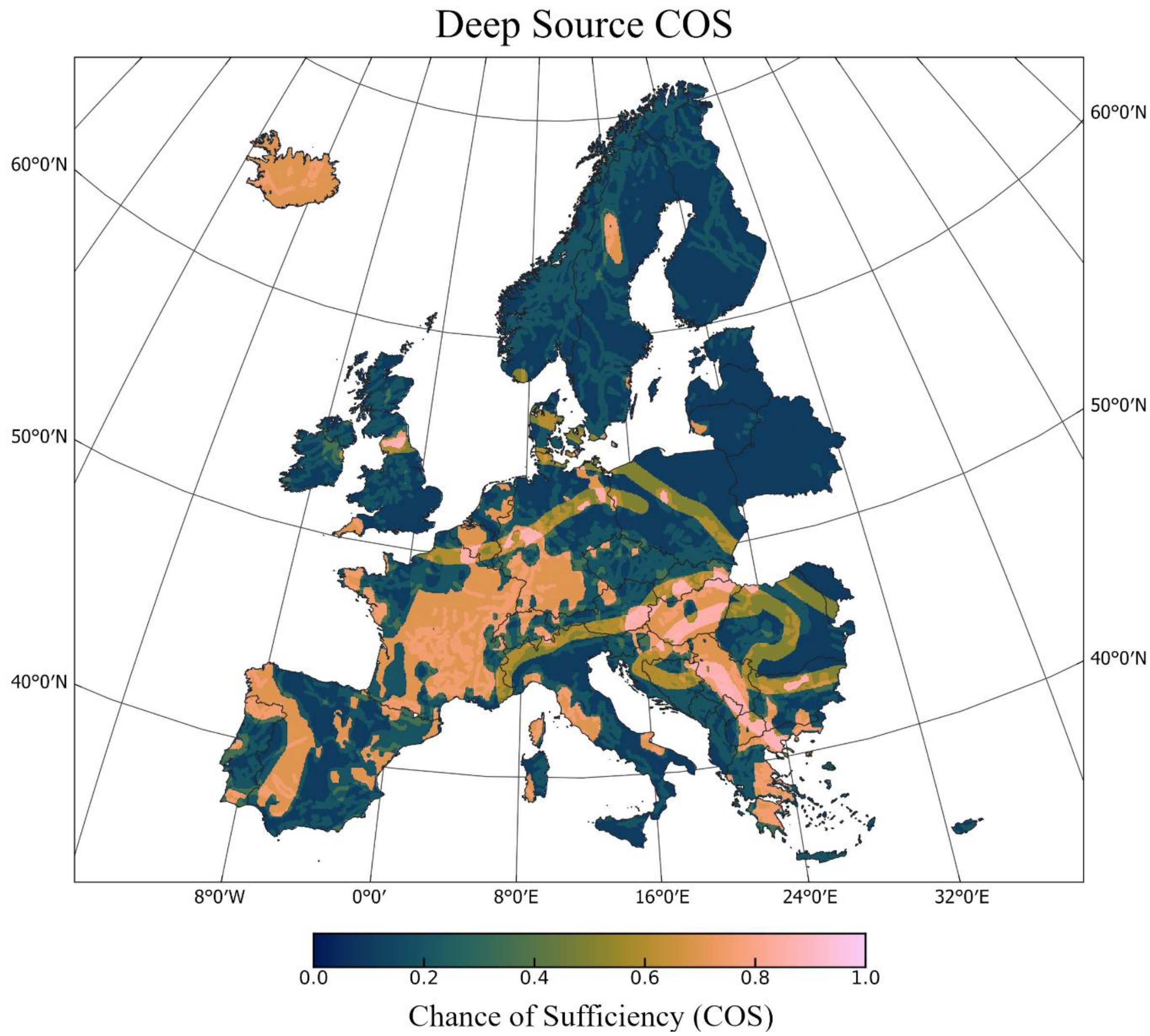

Figure 7 | *Composite COS map for deep source hydrogen potential, based on DEE1–DEE5*.

The three hydrogen source components—serpentinization, radiolysis, and deep-source processes—were integrated to produce a composite source map, shown in Figure 8. This layer reflects the overall chance of sufficiency (COS) for hydrogen generation across Europe, accounting for multiple geological processes and their respective indicators.

The influence of the East European Craton, a stable Precambrian geological unit, is clearly visible in the composite map due to its high radiolytic potential. Additionally, several Balkan countries display elevated COS values, highlighting regions with potentially favorable conditions for natural hydrogen generation. However, it is important to note that hydrogen generation alone is insufficient to define prospectivity. The viability of these regions depends on the presence of adequate reservoir and seal formations, which are addressed in the following section.

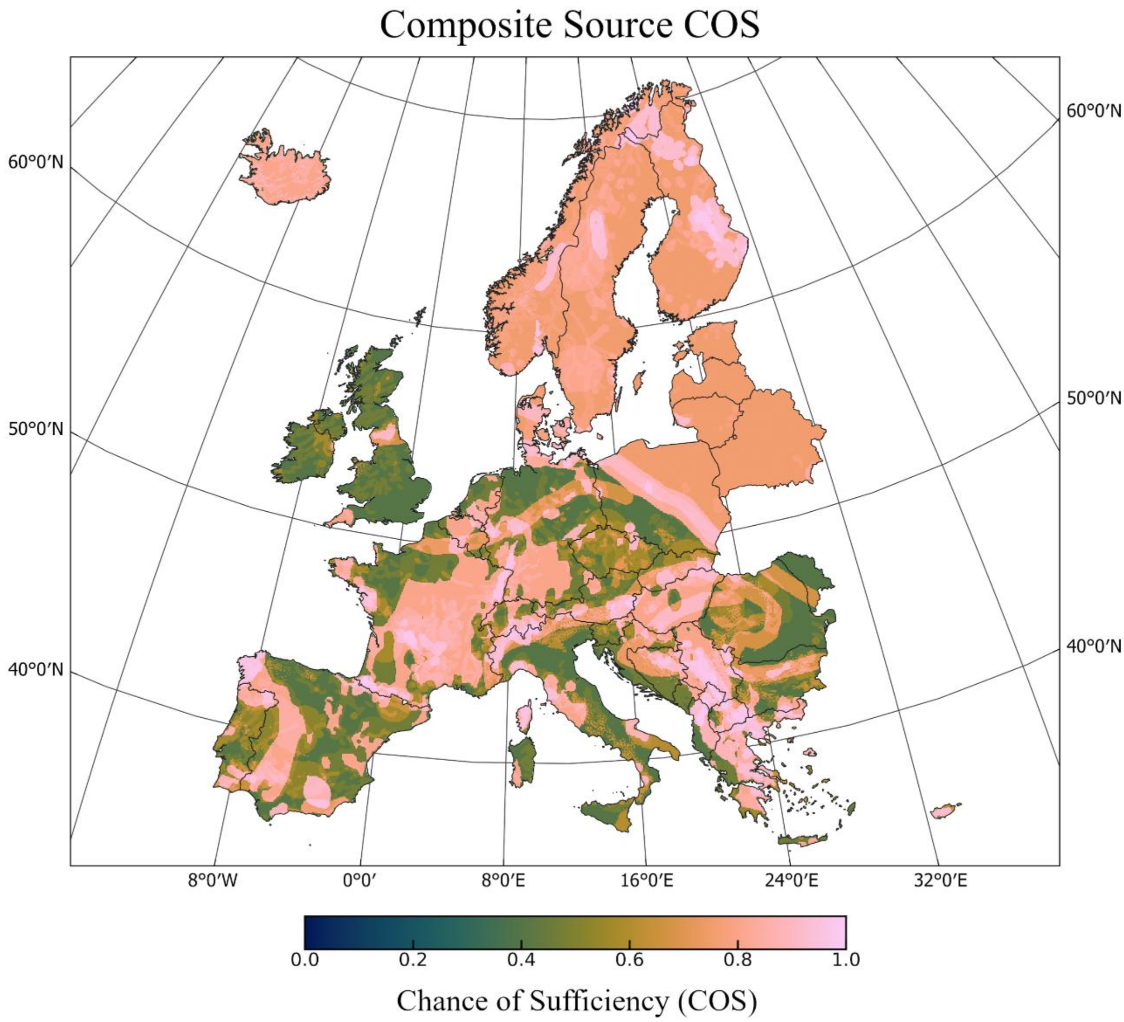

Figure 8 | *Composite COS map for hydrogen source potential, combining the serpentinization, radiolysis, and deep-source subcomponents.*

3.2 *Potential reservoirs*

For hydrogen to accumulate in economically viable quantities and contribute meaningfully to the energy transition, the presence of a porous and permeable reservoir is essential. Accordingly, sedimentary rocks, which typically exhibit such characteristics, are given higher COS values and are mapped in layer RES1 (Asch, 2005; Maiga, 2023). In contrast, layer RES2 represents igneous and metamorphic rocks, which generally exhibit lower porosity and are assigned lower COS values. Additionally, layer RES3 maps the extent of sedimentary basins, which are considered favourable due to their thick accumulations of sedimentary sequences that may host large-scale reservoirs (Gelman et al., 2025). These three reservoir-related indicators are shown in Figure 9, and their integration results in the composite reservoir COS map, displayed in Figure 10.

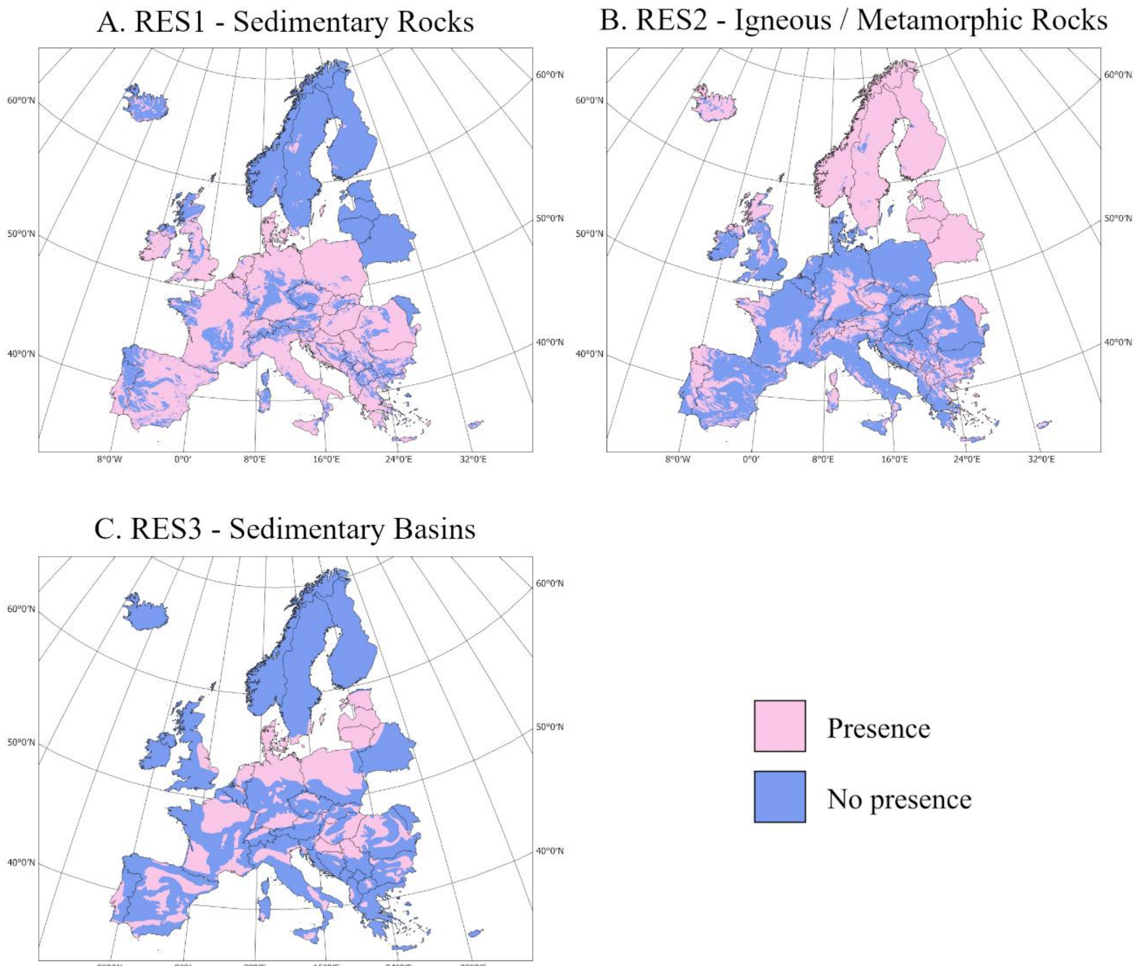

Figure 9 | *Geological indicators used for reservoir assessment (RES).* ***A:*** *Sedimentary rocks (RES1);* ***B:*** *Igneous/metamorphic rocks (RES2); C: Sedimentary basins (RES3). Data sources are listed in Table A.2 (Supplementary Materia).*

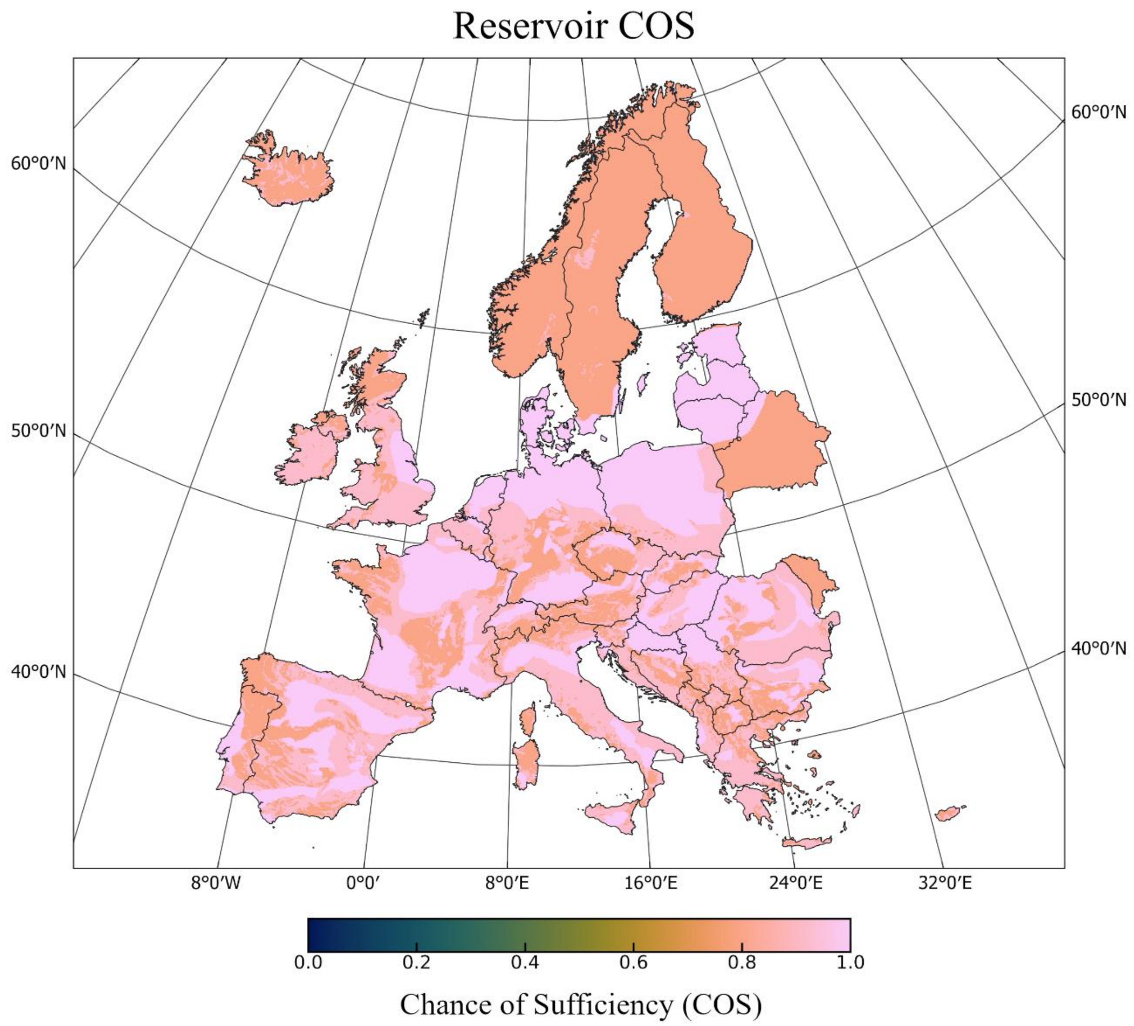

Figure 10 | *Composite COS map for reservoir suitability, based on layers RES1–RES3 and the COS values in Table 1.*

3.3 *Seals*

Effective hydrogen accumulation also requires a subsurface seal to prevent upward migration and escape to the atmosphere. The most effective of these are salt layers, mapped as SEA1, due to their extremely low permeability and proven sealing capabilities (Beauheim & Roberts, 2002). In addition, SEA2–SEA4 mirror the lithologies and structures used in the reservoir analysis (RES1–RES3), but with COS values adjusted to reflect their sealing potential (Gelman et al., 2025). Sedimentary rocks and basins, in particular, may contain interbedded shale or evaporite layers that can act as effective seals. These indicators are shown in Figure 11, and their integration yields the composite seal layer shown in Figure 12.

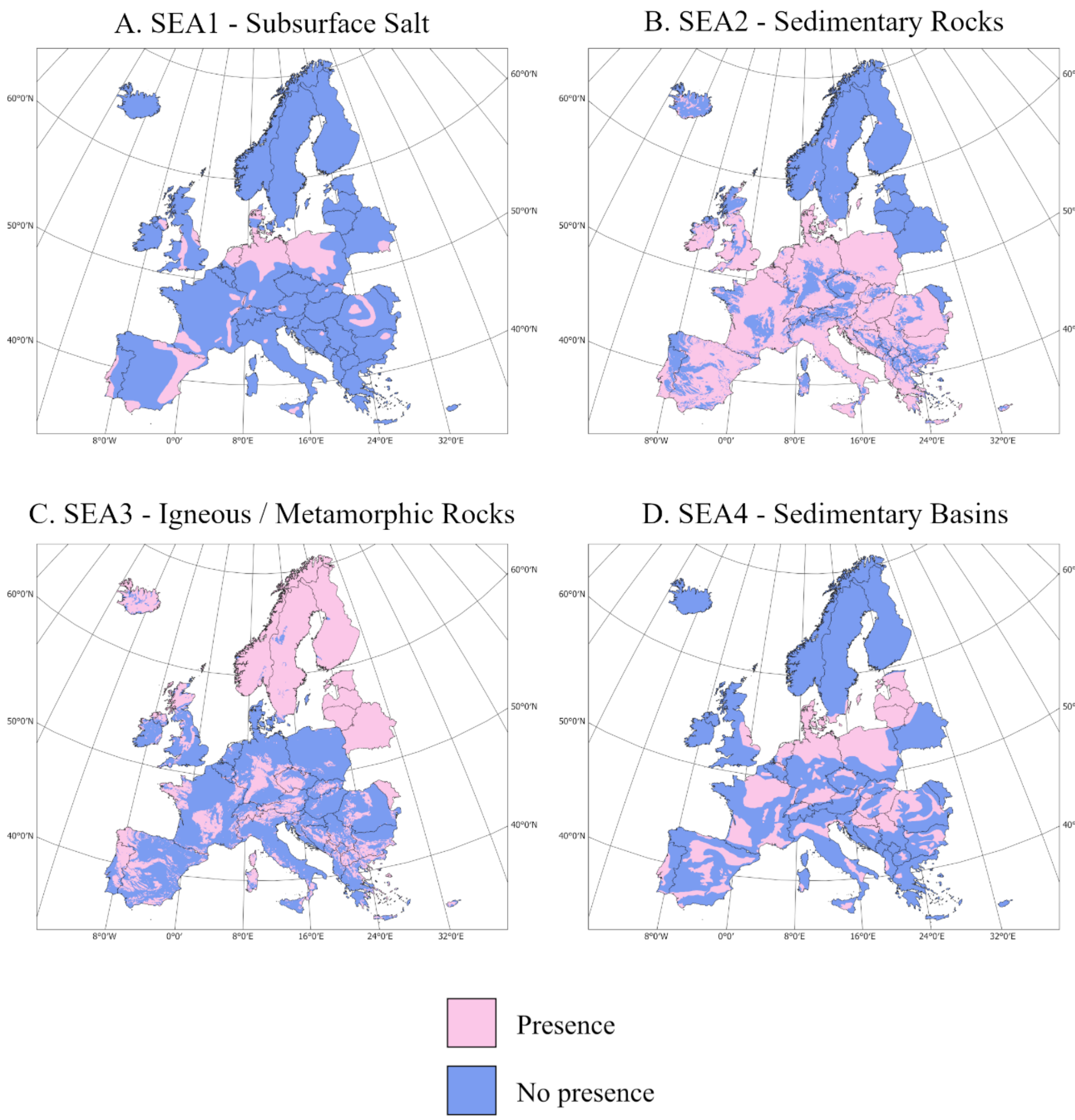

Figure 11 | *Geological indicators used for seal assessment (SEA).* ***A:*** *Subsurface salt (SEA1);* ***B:*** *Sedimentary rocks (SEA2);* ***C:*** *Igneous/metamorphic rocks (SEA3);* ***D:*** *Sedimentary basins (SEA4). Data sources are listed in Table A.2 (Supplementary Materia).*

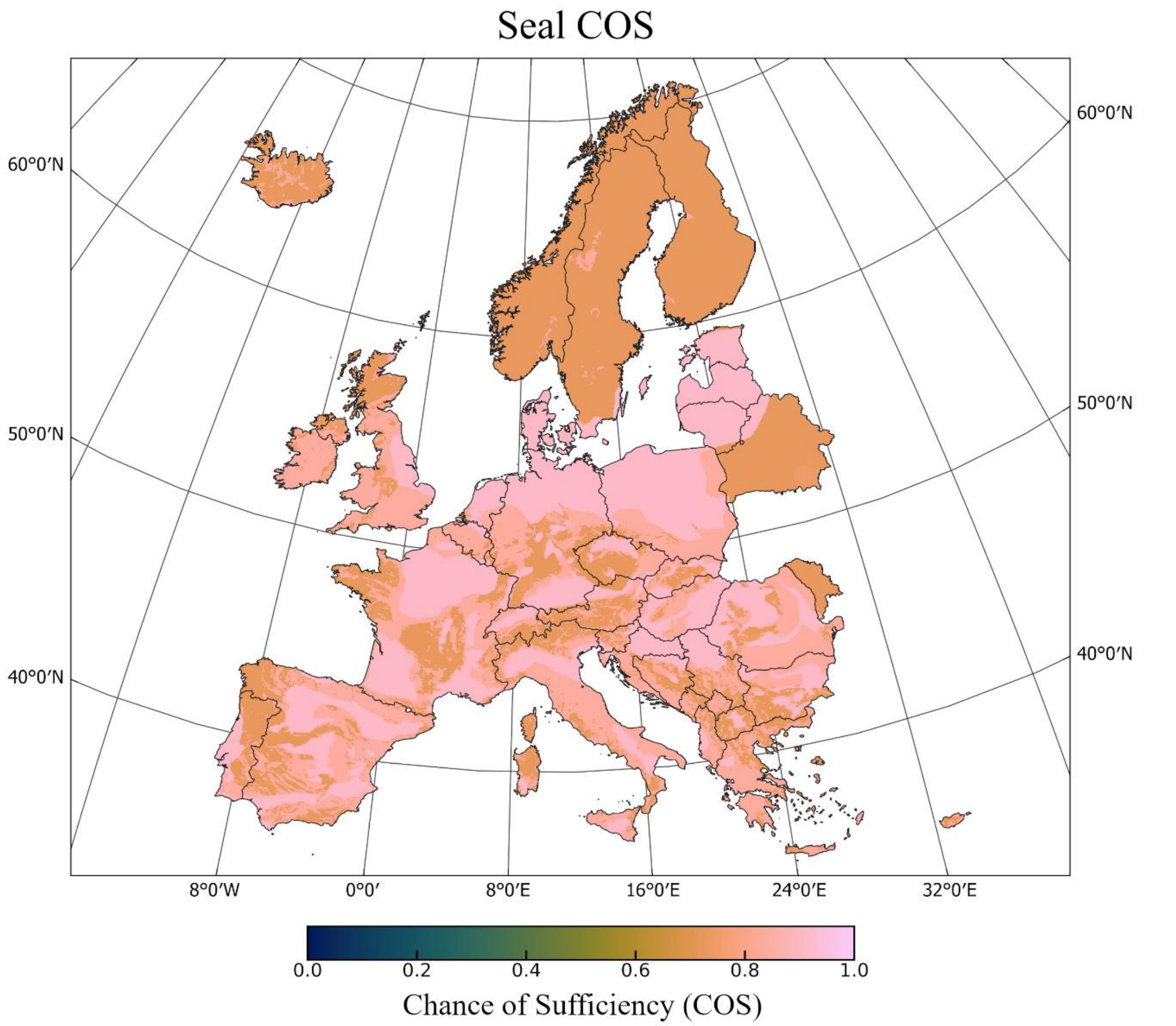

Figure 12 | *Composite COS map for seal potential, based on layers SEA1–SEA4 and COS values in Table 1*.

3.4 *Prospectivity of natural hydrogen*

The final prospectivity map (Figure 13) is produced by integrating the composite source, reservoir, and seal layers. This map represents the overall chance of sufficiency (COS) for hydrogen prospectivity across Europe, reflecting regions where hydrogen generation potential coincides with suitable trapping and storage conditions.

The highest prospectivity scores are identified in Poland, Denmark, Hungary, and Serbia. Other countries, including France and Germany, show moderate to high potential in localized regions. Notably, while Scandinavia exhibits a high source potential—primarily driven by radiolysis within the Precambrian craton—its overall prospectivity is moderated by lower COS values for reservoir and seal suitability.

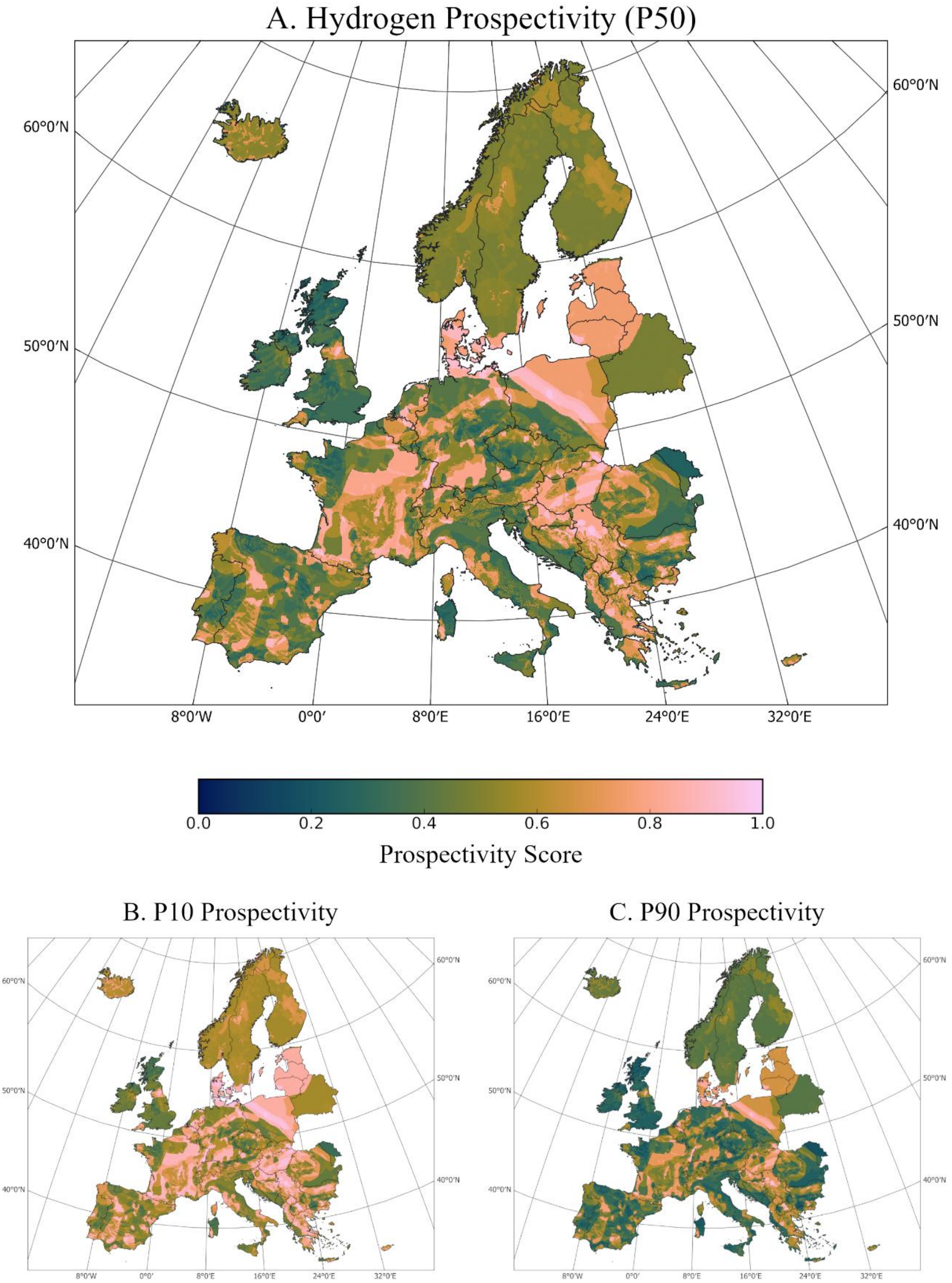

Figure 13 | *Final natural hydrogen prospectivity map, derived by integrating the composite source, reservoir, and seal layers using the methodology described in Section 2.*

3. 5 Validation against known hydrogen occurrences

To evaluate the reliability of the prospectivity model, the final map was compared with known natural hydrogen occurrences compiled from the literature (Table A.3). These occurrences are displayed in Figure 14, overlaid on the prospectivity map. For each documented occurrence, the maximum local prospectivity score (as derived from the P50 map in Figure 13) was extracted and recorded in Table A.3. The degree of spatial correlation between known hydrogen sites and regions of high predicted prospectivity provides qualitative support for the model's validity.

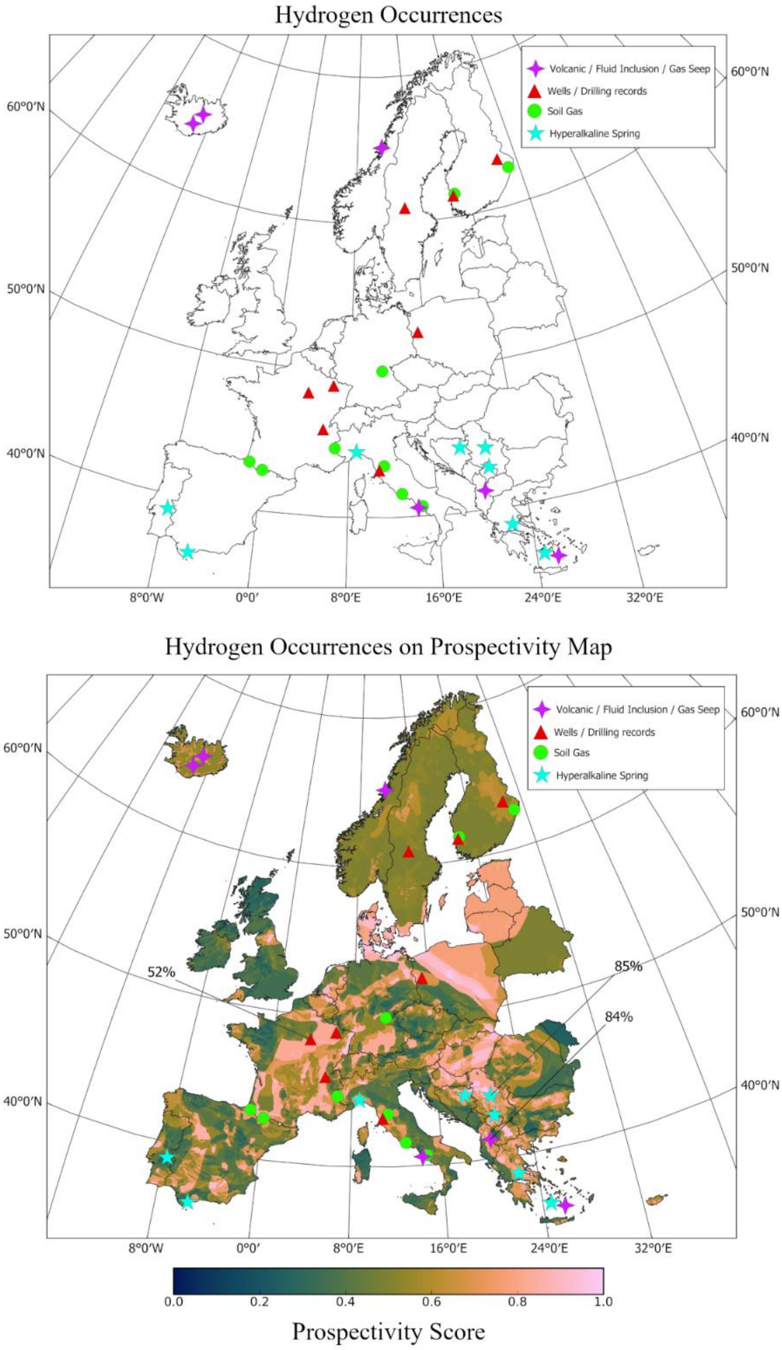

Figure 14 | *Comparison of known hydrogen occurrences (icons) with the final prospectivity map. Occurrence data sources are listed in Table A.3 (Supplementary Materia). The lower panel overlays occurrences on the COS map shown in Figure 13.*

A substantial number of documented natural hydrogen occurrences coincide with regions of high predicted prospectivity, particularly in Italy, the Balkans (e.g., Serbia, Albania), and Greece. Although Scandinavia displays a moderate overall prospectivity, the known occurrences there align with localized areas of elevated COS values. Conversely, some high-prospectivity regions—such as Denmark and Hungary—currently lack confirmed hydrogen occurrences, underscoring their potential as priority targets for future exploration and validation efforts.

4. Discussion

This study presents the first continent-scale natural hydrogen prospectivity map for Europe, integrating geological indicators of hydrogen generation, accumulation, and sealing. The map aligns well with recently documented occurrences of natural hydrogen, such as in Albania (Lévy et al., 2023), lending credibility to the methodology and underlying assumptions. By offering geological context for these occurrences, the results not only help explain observed hydrogen emissions but also highlight regions where generation potential coincides with viable reservoirs and seals.

Regions with the highest predicted prospectivity include Denmark, Hungary, France, Poland, North Macedonia, and Serbia. For some of these areas, hydrogen potential has already been recognized. For example, the Lorraine region of France was recently targeted in a 2024 exploration campaign (Meillaud & King, 2023; Waltham, 2024), and assessments are ongoing in Denmark (Geocenter Denmark, 2025). In contrast, other promising regions such as Hungary have received little to no attention in this context. The abundance of deep hydrogen source indicators and potential reservoir structures in Hungary suggest it should be prioritized in future field investigations.

Conversely, areas like Norway, Sweden, and Finland—despite exhibiting strong indicators for hydrogen generation (particularly radiolysis)—show moderate to low overall prospectivity. This is primarily due to the limited presence of sedimentary reservoirs and sealing formations across the Fennoscandian Shield, where crystalline basement rocks dominate (Rosberg & Erlström, 2021). This contrasts with findings from North America, where radiolytic hydrogen in cratonic settings is considered more viable due to the presence of thick sedimentary cover (Marshak & van der Pluijm, 2020; Gelman et al., 2025). Nevertheless, recent research suggests that in-situ hydrogen generation via geological stimulation of ultramafic rocks may offer a path forward even in shield regions (Templeton et al., 2024). The compilation of ultramafic bodies provided in this study (Supplementary Material A.1) can therefore serve not only for passive exploration but also as a guide for potential stimulation-based approaches.

This study is subject to several limitations. First, offshore areas were excluded, despite their significant potential. For instance, the failed rift basins beneath the North Sea—characterized by thick sedimentary sequences and abundant salt structures—may present ideal conditions for hydrogen generation, migration, and trapping (Rattey & Hayward, 1999). Second, hydrogen migration processes were not explicitly modelled. Subsurface migration is critical for understanding accumulation potential, especially in faulted or rifted terrains. Previous studies have successfully applied hydrocarbon-based flow path models to hydrogen (Gelman et al., 2025), and numerical simulations have demonstrated fault-facilitated hydrogen transport (Donzé et al., 2022). Integrating such migration models with offshore data would provide a more complete prospectivity assessment.

Advancements in remote sensing and machine learning also offer promising avenues for improving exploration efficiency. Algorithms trained on surface expressions of hydrogen (e.g., vegetation anomalies, gas seepage signatures) could help refine subsurface targeting in high-COS regions identified in this study (Ohio State University, 2023).

Finally, this analysis relied on Europe-wide datasets, which, while suitable for a first-order screening study, vary in quality and resolution. These compilations often reflect heterogeneous national datasets with differing classification standards, completeness, and scale. As such, detailed national-scale analyses in high-prospectivity countries—particularly those currently underexplored—are essential next steps. Expanding and standardizing datasets on key parameters, such as subsurface uranium distribution, would greatly enhance the resolution and reliability of future continent-wide assessments.

5. Conclusions

This study presents the first continent-scale prospectivity assessment for natural hydrogen in Europe, offering a foundational spatial framework for early-stage exploration. By integrating indicators of hydrogen generation—through serpentinization, radiolysis, and deep-sourced processes—with assessments of potential reservoirs and sealing formations, a comprehensive map of relative hydrogen prospectivity was developed.

A novel element of this work is the systematic compilation of ultramafic rock bodies across Europe, serving as a critical input for evaluating serpentinization potential. The integration of multiple geological datasets and Monte Carlo-based uncertainty modelling enabled the identification of several high-prospectivity regions, most notably in Hungary, Denmark, Poland, Serbia, and parts of France and North Macedonia. These results are consistent with many known hydrogen occurrences and also highlight underexplored regions where field validation and further research are urgently warranted.

While the study focuses on onshore areas and does not incorporate dynamic hydrogen migration models, it provides a crucial first-order screening tool. The methodology and datasets developed here can be used as a basis for more detailed national assessments and support future incorporation of offshore data, geochemical modelling, and migration pathway simulations.

In the context of the energy transition, natural hydrogen represents a potentially low-cost, carbon-free energy source. Its viability will ultimately depend on resource accessibility, renewability, regulatory frameworks, and technological developments in detection, stimulation, and extraction. By identifying regions where favourable geological conditions overlap, this study supports strategic exploration planning and emphasizes Europe’s potential to harness natural hydrogen as part of a broader transition toward sustainable and secure energy systems.

CRediT statement

FHJW: Methodology, software, formal analysis, investigation, visualisation, writing original draft.
JMM: Conceptualisation, supervision, writing – review & editing.

References

Aertgeerts, G. (2016). Étude pétrologique des reliques ophiolitiques des complexes de Champtoceaux et d'Audierne : caractérisation des minéraux fibreux dans les roches mafiques et ultramafiques. http://hal.univ-nantes.fr/tel-01286275v1

Aimar, L., Frery, E., Strand, J., Heath, C., Khan, S., Moretti, I., & Ong, C. (2023). Natural hydrogen seeps or salt lakes: how to make a difference? Grass Patch example, Western Australia. Frontiers in Earth Science, 11. https://doi.org/10.3389/feart.2023.1236673

Allard, P., Maiorani, A., Tedesco, D., Cortecci, G., & Turi, B. (1991). Isotopic study of the origin of sulfur and carbon in Solfatara fumaroles, Campi Flegrei caldera. Journal of Volcanology and Geothermal Research, 48(1–2), 139–159. https://doi.org/10.1016/0377-0273(91)90039-3

Asch, K. (2005). International Geological Map of Europe and Adjacent Areas 1 : 5 000 000 (IGME5000) [Geological map]. Bundesanstalt für Geowissenschaften und Rohstoffe; Commission for the Geological Map of the World. https://doi.org/10.25928/igme-5000

Balen, D., & Massonne, H. (2021). Two contrasting P-T paths for metamorphic sole amphibolites of the Dinaride Ophiolite Zone (Krivaja-Konjuh ultramafic massif, Central Bosnia and Herzegovina) and their geodynamic implications. Lithos, 394–395, 106184. https://doi.org/10.1016/j.lithos.2021.106184

Ballentine, C.J., Karolytė, R., Cheng, A. et al. Natural hydrogen resource accumulation in the continental crust. Nat Rev Earth Environ 6, 342–356 (2025). https://doi.org/10.1038/s43017-025-00670-1

Bazylev, B. A., Karamata, S., & Zakariadze, G. S. (2003). Petrology and evolution of the Brezovica ultramafic massif, Serbia. Geological Society London Special Publications, 218(1), 91–108. https://doi.org/10.1144/gsl.sp.2003.218.01.06

Beqiraj, A. (2000). Geochemical Characterization of Podiform Chromite Ores from the Ultramafic Massif of Bulqiza (Eastern Ophiolitic Belt, Albania) and Hints for Exploration. Exploration and Mining Geology, 9(2), 149–156. https://doi.org/10.2113/0090149

Berger, J., Femenias, O., Mercier, J. C. C., & Demaiffe, D. (2005). Ocean-floor hydrothermal metamorphism in the Limousin ophiolites (western French Massif Central): evidence of a rare preserved Variscan oceanic marker. Journal of Metamorphic Geology, 23(9), 795–812. https://doi.org/10.1111/j.1525-1314.2005.00610.x

Bermejo, R. M. B., Ramírez, P. B., De Balbín Behrmann, R., & De Los Ángeles Lancharro Gutiérrez, M. (2017). Production and consumption of salt in the inland Tagus Valley in Prehistory (Spain). KEY RESOURCES AND SOCIO- CULTURAL DEVELOPMENTS IN THE IBERIAN CHALCOLITHIC, 89–105. https://dx.doi.org/10.15496/publikation-19737

Bicocchi, G., Tassi, F., Bonini, M., Capecchiacci, F., Ruggieri, G., Buccianti, A., Burgassi, P., & Vaselli, O. (2013). The high pCO2 Caprese Reservoir (Northern Apennines, Italy): Relationships between present- and paleo-fluid geochemistry and structural setting. Chemical Geology, 351, 40–56. https://doi.org/10.1016/j.chemgeo.2013.05.001

Blanco, H., & Faaij, A. (2017). A review at the role of storage in energy systems with a focus on Power to Gas and long-term storage. Renewable and Sustainable Energy Reviews, 81, 1049–1086. https://doi.org/10.1016/j.rser.2017.07.062

Boev, B., Cvetković, V., Prelević, D., Šarić, K., & Boev, I. (2018). EAST VARDAR OPHIOLITES REVISITED: A BRIEF SYNTHESIS OF GEOLOGY AND GEOCHEMICAL DATA. Contributions Section of Natural Mathematical and Biotechnical Sciences, 39(1), 51. https://doi.org/10.20903/csnmbs.masa.2018.39.1.119

Bogatu, A., Giselle, S., Tremblay, A., Meshi, A., & Bédard, J. (2019). Western- and Eastern-type ultramafic massifs of the Mirdita ophiolite, Albania: structural evidence for lower-plate (Western-type) - upper-plate (Eastern-type) relationships and formation of a Jurassic oceanic core complex. EGUGA, 11952. http://ui.adsabs.harvard.edu/abs/2019EGUGA..2111952B/abstract

Bonnemains, D., Carlut, J., Escartín, J., Mével, C., Andreani, M., & Debret, B. (2016). Magnetic signatures of serpentinization at ophiolite complexes. Geochemistry Geophysics Geosystems, 17(8), 2969–2986. https://doi.org/10.1002/2016gc006321

Bonvalot, S., Briais, A., Kuhn, M., Peyrefitte, A., Vales, N., Biancale, R., Gabalda, G., Moreaux, G., Reinquin, F. & Sarrailh, M. (2012). Global grids : World Gravity Map (WGM2012). Bureau Gravimetrique International. https://doi.org/10.18168/bgi.23

Brunet, F., Malvoisin, B. (2025). Can natural H2 be considered renewable? The reference case of a deep aquifer in an intracratonic sedimentary basin. Advances in Geochemistry and Cosmochemistry 1(2), 738-738. https://doi.org/10.33063/agc.v1i2.738

Byrd Polar & Climate Research Center. (2023, December 30). AI mapping reveals potential subsurface natural hydrogen worldwide. The Ohio State University. Retrieved June 14, 2025, from https://byrd.osu.edu/news/ai-mapping-reveals-potential-subsurface-natural-hydrogen-worldwide

Caglayan, D. G., Weber, N., Heinrichs, H. U., Linßen, J., Robinius, M., Kukla, P. A., & Stolten, D. (2020). Technical potential of salt caverns for hydrogen storage in Europe. International Journal of Hydrogen Energy, 45(11), 6793–6805. https://doi.org/10.1016/j.ijhydene.2019.12.161

Campbell, S. D. G., Howells, M. F., Smith, M., & Reedman, A. J. (1988). A Caradoc Failed-Rift within the Ordovician Marginal Basin of Wales. Geological Magazine, 125(3), 257–266. https://doi.org/10.1017/s0016756800010190

Canérot, J. (2017). The pull apart-type Tardets-Mauléon Basin, a key to understand the formation of the Pyrenees. BSGF – Earth Sciences Bulletin, 188(6), 35. https://doi.org/10.1051/bsgf/2017198

Carapezza, M. L., & Tarchini, L. (2007). Accidental gas emission from shallow pressurized aquifers at Alban Hills volcano (Rome, Italy): Geochemical evidence of magmatic degassing? Journal of Volcanology and Geothermal Research, 165(1–2), 5–16. https://doi.org/10.1016/j.jvolgeores.2007.04.008

CGS Europe. (2013). Pan-European coordination action on CO_2 geological storage. European Commission. Retrieved from https://cordis.europa.eu/project/id/256725

Chamorro, C. R., García-Cuesta, J. L., Mondéjar, M. E., & Pérez-Madrazo, A. (2013). Enhanced geothermal systems in Europe: An estimation and comparison of the technical and sustainable potentials. Energy, 65, 250–263. https://doi.org/10.1016/j.energy.2013.11.078

Chavagnac, V., Ceuleneer, G., Monnin, C., Lansac, B., Hoareau, G., & Boulart, C. (2013). Mineralogical assemblages forming at hyperalkaline warm springs hosted on ultramafic rocks: A case study of Oman and Ligurian ophiolites. Geochemistry Geophysics Geosystems, 14(7), 2474–2495. https://doi.org/10.1002/ggge.20146

Chiodini, G., Frondini, F., Cardellini, C., Granieri, D., Marini, L., & Ventura, G. (2001). CO2 degassing and energy release at Solfatara volcano, Campi Flegrei, Italy. Journal of Geophysical Research Atmospheres, 106(B8), 16213–16221. https://doi.org/10.1029/2001jb000246

Cloetingh, S., & Cornu, T. (2005). Neotectonics and Quaternary fault-reactivation in Europe's intraplate lithosphere. Elsevier. https://research.vu.nl/en/publications/neotectonics-and-quaternary-fault-reactivation-in-europes-intrapl

Collins, L. (2023, May 16). "Significant concentrations" of natural hydrogen discovered in northeast France by local power and gas producer. hydrogeninsight.com. https://www.hydrogeninsight.com/production/significant-concentrations-of-natural-hydrogen-discovered-in-northeast-france-by-local-power-and-gas-producer/2-1-1452270

Combaudon, V., Moretti, I., Kleine, B. I., & Stefánsson, A. (2022). Hydrogen emissions from hydrothermal fields in Iceland and comparison with the Mid-Atlantic Ridge. International Journal of Hydrogen Energy, 47(18), 10217–10227. https://doi.org/10.1016/j.ijhydene.2022.01.101

Criss, R. E. (2019). Thermal models of the continental lithosphere. In Elsevier eBooks (pp. 151–174). https://doi.org/10.1016/b978-0-12-818430-1.00006-9

Daae, F. L., Økland, I., Dahle, H., Jørgensen, S. L., Thorseth, I. H., & Pedersen, R. B. (2013). Microbial life associated with low-temperature alteration of ultramafic rocks in the Leka ophiolite complex. Geobiology, 11(4), 318–339. https://doi.org/10.1111/gbi.12035

Daskalopoulou, K., Gagliano, A. L., Calabrese, S., Longo, M., Hantzis, K., Kyriakopoulos, K., & D'Alessandro, W. (2018). Gas geochemistry and CO2 output estimation at the island of Milos, Greece. Journal of Volcanology and Geothermal Research, 365, 13–22. https://doi.org/10.1016/j.jvolgeores.2018.10.003

De Hoog, J. C., Janák, M., Vrabec, M., & Froitzheim, N. (2008). Serpentinised peridotites from an ultrahigh-pressure terrane in the Pohorje Mts. (Eastern Alps, Slovenia): Geochemical constraints on petrogenesis and tectonic setting. Lithos, 109(3–4), 209–222. https://doi.org/10.1016/j.lithos.2008.05.006

Deronzier, J., & Giouse, H. (2020). Vaux-en-Bugey (Ain, France): the first gas field produced in France, providing learning lessons for natural hydrogen in the sub-surface? BSGF – Earth Sciences Bulletin, 191, 7. https://doi.org/10.1051/bsgf/2020005

Deville, E., & Prinzhofer, A. (2016). The origin of N2-H2-CH4-rich natural gas seepages in ophiolitic context: A major and noble gases study of fluid seepages in New Caledonia. Chemical Geology, 440, 139–147. https://doi.org/10.1016/j.chemgeo.2016.06.011

Donzé, F., Bourdet, L., Truche, L., Taillefer, A., Dutoit, H., Dusseaux, C., & Lefeuvre, N. (2022). Numerical modeling of natural hydrogen migration from deep sources within fault zones. Goldschmidt Abstracts. https://doi.org/10.46427/gold2022.10924

Donzé, F., Lefeuvre, N., Truche, L., Yao, Y., Vujevíc, I., & Dutoit, H. (2024). Natural hydrogen exploration within western European and eastern Mediterranean ophiolites and ultramafic complexes. Geochemistry Exploration Environment Analysis. https://doi.org/10.1144/geochem2024-043

Dugamin E., Truche L., Donzé F.V. (2019). Natural Hydrogen Exploration Guide, Geonum Ed.: ISRN GEONUM-NST--2019-01--ENG, 16 pages.

Dèzes, P., Schmid, S., & Ziegler, P. (2004). Evolution of the European Cenozoic Rift System: interaction of the Alpine and Pyrenean orogens with their foreland lithosphere. Tectonophysics, 389(1–2), 1–33. https://doi.org/10.1016/j.tecto.2004.06.011

Ellis, G. S., & Gelman, S. E. (2024). Model predictions of global geologic hydrogen resources. Science Advances, 10(50). https://doi.org/10.1126/sciadv.ado0955

Escartín, J., & Cannat, M. (1999). Ultramafic exposures and the gravity signature of the lithosphere near the Fifteen-Twenty Fracture Zone (Mid-Atlantic Ridge, 14°–16.5°N). Earth and Planetary Science Letters, 171(3), 411–424. https://doi.org/10.1016/s0012-821x(99)00169-7

Etiope, G. (2024). Natural hydrogen extracted from ophiolitic rocks: A first dataset. International Journal of Hydrogen Energy, 78, 368–372. https://doi.org/10.1016/j.ijhydene.2024.06.292

Etiope, G., Samardžić, N., Grassa, F., Hrvatović, H., Miošić, N., & Skopljak, F. (2017). Methane and hydrogen in hyperalkaline groundwaters of the serpentinized Dinaride ophiolite belt, Bosnia and Herzegovina. Applied Geochemistry, 84, 286–296. https://doi.org/10.1016/j.apgeochem.2017.07.006

Etiope, G., Vadillo, I., Whiticar, M., Marques, J., Carreira, P., Tiago, I., Benavente, J., Jiménez, P., & Urresti, B. (2015). Abiotic methane seepage in the Ronda peridotite massif, southern Spain. Applied Geochemistry, 66, 101–113. https://doi.org/10.1016/j.apgeochem.2015.12.001

EuroGeoSurveys EGDI Operations Group. (2021, September 1). MIN4EU harmonized dataset – "Minerals Inventory" [Web Map Service]. EGDI Spatial Metadata Catalogue. https://www.europe-geology.eu/mineral-resources/

Fejza, I., Avdullahi, S., Meshi, A., Meha, M., & Tmava, A. (2010). Ultrabasic Massif of Goleshi (Kosova): Microstructural and Kinematic Analysis. Online Journal of Earth Sciences, 4(1), 6–12. https://doi.org/10.3923/ojesci.2010.6.12

Fejza, I., Shala, A., Kutllovci, F., & Tmava, A. (2022). Petrographic and geochemical characteristics of rocks in the Drenas region, Kosovo. Mining of Mineral Deposits, 16(2), 110–115. https://doi.org/10.33271/mining16.02.110

Flinn, D. (2001). The basic rocks of the Shetland Ophiolite Complex and their bearing on its genesis. Scottish Journal of Geology, 37(2), 79–96. https://doi.org/10.1144/sjg37020079

Fraefel, M. (2008). Geomorphic response to neotectonic activity in the Jura Mountains and in the southern Upper Rhine Graben. https://doi.org/10.5451/unibas-004757231

Frassi, C., Musumeci, G., Zucali, M., Mazzarini, F., Rebay, G., & Langone, A. (2017). The Cotoncello Shear Zone (Elba Island, Italy): The deep root of a fossil oceanic detachment fault in the Ligurian ophiolites. Lithos, 278–281, 445–463. https://doi.org/10.1016/j.lithos.2017.02.015

Frery, E., Langhi, L., Maison, M., & Moretti, I. (2021). Natural hydrogen seeps identified in the North Perth Basin, Western Australia. International Journal of Hydrogen Energy, 46(61), 31158–31173. https://doi.org/10.1016/j.ijhydene.2021.07.023

Fuel cell works. (2024, October 21). Natural hydrogen, helium found in Finland by 80 Mile Plc | Fuel Cells works. https://fuelcellsworks.com/2024/10/21/green-hydrogen/80-mile-plc-discovers-natural-hydrogen-helium-at-hammaslahti-project-in-finland

Féménias, O., Coussaert, N., Bingen, B., Whitehouse, M., Mercier, J. C., & Demaiffe, D. (2003). A Permian underplating event in late- to post-orogenic tectonic setting. Evidence from the mafic–ultramafic layered xenoliths from Beaunit (French Massif Central). Chemical Geology, 199(3–4), 293–315. https://doi.org/10.1016/s0009-2541(03)00124-4

Gaucher, E. C., Moretti, I., Pélissier, N., Burridge, G., & Gonthier, N. (2023). The place of natural hydrogen in the energy transition: A position paper. Zenodo (CERN European Organization for Nuclear Research). https://doi.org/10.5281/zenodo.8108239

Gee, D. G., & Stephenson, R. A. (2006). The European lithosphere: an introduction. Geological Society London Memoirs, 32(1), 1–9. https://doi.org/10.1144/gsl.mem.2006.032.01.01

Gelman, S. E., Hearon, J. S., & Ellis, G. S. (2025). Prospectivity mapping for geologic hydrogen. USGS Professional Paper. https://doi.org/10.3133/pp1900

George, R. P. (1978). Structural petrology of the Olympus ultramafic complex in the Troodos ophiolite, Cyprus. Geological Society of America Bulletin, 89(6), 845. https://doi.org/10.1130/0016-7606(1978)89

Gillard, M., Tugend, J., Müntener, O., Manatschal, G., Karner, G. D., Autin, J., Sauter, D., Figueredo, P. H., & Ulrich, M. (2019). The role of serpentinization and magmatism in the formation of decoupling interfaces at magma-poor rifted margins. Earth-Science Reviews, 196, 102882. https://doi.org/10.1016/j.earscirev.2019.102882

González-Pérez, I., Fanlo, I., Ares, G., Gervilla, F., González-Jiménez, J. M., Acosta-Vigil, A., & Arranz, E. (2023). The unconventional Peridotite-Related MG-FE-B Skarn of the El Robledal, SE Spain. Minerals, 13(3), 300. https://doi.org/10.3390/min13030300

Handy, M. R., Giese, J., Schmid, S. M., Pleuger, J., Spakman, W., Onuzi, K., & Ustaszewski, K. (2019). Coupled Crust-Mantle response to slab tearing, bending, and rollback along the Dinaride-Hellenide orogen. Tectonics, 38(8), 2803–2828. https://doi.org/10.1029/2019tc005524

Havlíček, F., Uličný, D., Krýza, O., Machek, M., Warsitzka, M., and Závada, P. (2024). Modelling the effects of changing extension directions in a segmented rift: application to the Eger Rift, Central Europe, EGU General Assembly 2024, Vienna, Austria, EGU24-9770, https://doi.org/10.5194/egusphere-egu24-9770

Heggie, G., Barnes, S., & Fiorentini, M. (2013). Application of lithogeochemistry in the assessment of nickel-sulphide potential in komatiite belts from northern Finland and Norway. Bulletin of the Geological Society of Finland, 85(2), 107–126. https://doi.org/10.17741/bgsf/85.2.001

Hunt, T. (1978). Interpretation of gravity anomalies over the Dun Mountain ultramafic body (Note). New Zealand Journal of Geology and Geophysics, 21(3), 413–417. https://doi.org/10.1080/00288306.1978.10424065

INSPIRE, Temporary MIWP 2021–2024 sub-group 2.3.1. (2024, July 31). D2.8.III.21 Data specification on mineral resources – Technical guidelines (Version 3.0.0). INSPIRE Maintenance and Implementation Group (MIG). https://inspire.ec.europa.eu/id/document/tg/mr

Jackson, O., Lawrence, S. R., Hutchinson, I. P., Stocks, A. E., Barnicoat, A. C., & Powney, M. (2024). Natural hydrogen: sources, systems and exploration plays. Geoenergy, 2(1). https://doi.org/10.1144/geoenergy2024-002

Jesus, A. P., Munhá, J., Mateus, A., Tassinari, C., & Nutman, A. P. (2007). The Beja Layered Gabbroic Sequence (Ossa-Morena Zone, Southern Portugal): geochronology and geodynamic implications. Geodinamica Acta, 20(3), 139–157. https://doi.org/10.3166/ga.20.139-157

Jin, Z., Zhang, P., Liu, R., Huang, X., Wang, X., Meng, Q., Liu, J., Su, Y., & Zhang, H. (2024). Discovery of anomalous hydrogen leakage sites in the Sanshui Basin, South China. Science Bulletin, 69(9), 1217–1220. https://doi.org/10.1016/j.scib.2024.03.002

Khogenkumar, S., Singh, A. K., Singh, R. B., Khanna, P., Singh, N. I., & Singh, W. I. (2015). Coexistence of MORB and OIB-type mafic volcanics in the Manipur Ophiolite Complex, Indo-Myanmar Orogenic Belt, northeast India: Implication for heterogeneous mantle source at the spreading zone. Journal of Asian Earth Sciences, 116, 42–58. https://doi.org/10.1016/j.jseaes.2015.11.007

Klein, F., Bach, W., & McCollom, T. M. (2013). Compositional controls on hydrogen generation during serpentinization of ultramafic rocks. Lithos, 178, 55–69. https://doi.org/10.1016/j.lithos.2013.03.008

Konnunaho, J., Hanski, E., Wing, B., Bekker, A., Lukkari, S., & Halkoaho, T. (2015). The Hietaharju PGE-enriched komatiite-hosted sulfide deposit in the Archean Suomussalmi greenstone belt, eastern Finland. Ore Geology Reviews, 72, 641–658. https://doi.org/10.1016/j.oregeorev.2015.08.022

Kousksou, T., Bruel, P., Jamil, A., Rhafiki, T. E., & Zeraouli, Y. (2013). Energy storage: Applications and challenges. Solar Energy Materials and Solar Cells, 120, 59–80. https://doi.org/10.1016/j.solmat.2013.08.015

Kryza, R., & Pin, C. (2009). The Central-Sudetic ophiolites (SW Poland): Petrogenetic issues, geochronology and palaeotectonic implications. Gondwana Research, 17(2–3), 292–305. https://doi.org/10.1016/j.gr.2009.11.001

Kumar, K. R., Makhmutov, A., Spiers, C. J., & Hajibeygi, H. (2021). Geomechanical simulation of energy storage in salt formations. Scientific Reports, 11(1). https://doi.org/10.1038/s41598-021-99161-8

Kübler, S., Streich, R., Lück, E., Hoffmann, M., Friedrich, A. M., & Strecker, M. R. (2016). Active faulting in a populated low-strain setting (Lower Rhine Graben, Central Europe) identified by geomorphic, geophysical and geological analysis. Geological Society London Special Publications, 432(1), 127–146. https://doi.org/10.1144/sp432.11

Langhi, L., & Strand, J. (2023b). Exploring natural hydrogen hotspots: a review and soil-gas survey design for identifying seepage. Geoenergy, 1(1). https://doi.org/10.1144/geoenergy2023-014

Lefeuvre, N., Thomas, E., Truche, L., Donzé, F., Cros, T., Dupuy, J., Pinzon-Rincon, L., & Rigollet, C. (2024). Characterizing natural hydrogen occurrences in the Paris Basin from historical drilling records. Geochemistry Geophysics Geosystems, 25(5). https://doi.org/10.1029/2024gc011501

Lefeuvre, N., Truche, L., Donzé, F., Ducoux, M., Barré, G., Fakoury, R., Calassou, S., & Gaucher, E. C. (2021). Native H2 exploration in the western Pyrenean foothills. Geochemistry Geophysics Geosystems, 22(8). https://doi.org/10.1029/2021gc009917

Lefeuvre, N., Truche, L., Donzé, F., Gal, F., Tremosa, J., Fakoury, R., Calassou, S., & Gaucher, E. (2022). Natural hydrogen migration along thrust faults in foothill basins: The North Pyrenean Frontal Thrust case study. Applied Geochemistry, 145, 105396. https://doi.org/10.1016/j.apgeochem.2022.105396

Leshukov, T., Legoshchin, K., Avdeev, K., Baranova, E., & Larionov, A. (2024). Depth gradient and radon activity concentration in soil gas in the zone of a potentially active fault. Earth, 5(4), 1005–1022. https://doi.org/10.3390/earth5040052

Liebreich, M. (2023, October 20). Hydrogen Ladder Version 5.0. LinkedIn. https://www.linkedin.com/pulse/hydrogen-ladder-version-50-michael-liebreich

Liipo, J., Vuollo, J., Nykänen, V., Piirainen, T., Pekkarinen, L., & Tuokko, I. (1995). Chromites from the early Proterozoic Outokumpu-Jormua Ophiolite Belt: a comparison with chromites from Mesozoic ophiolites. Lithos, 36(1), 15–27. https://doi.org/10.1016/0024-4937(95)00002-w

Liu, J., Liu, Q., Xu, H., Ding, Q., Zhu, D., & Meng, Q. (2023). Genesis and energy significance of natural hydrogen. Unconventional Resources, 3, 176–182. https://doi.org/10.1016/j.uncres.2023.01.002

Lollar, B. S., Onstott, T. C., Lacrampe-Couloume, G., & Ballentine, C. J. (2014). The contribution of the Precambrian continental lithosphere to global H2 production. Nature, 516(7531), 379–382. https://doi.org/10.1038/nature14017

Lollar, B. S., Voglesonger, K., Lin, L., Lacrampe-Couloume, G., Telling, J., Abrajano, T., Onstott, T., & Pratt, L. (2007). Hydrogeologic Controls on Episodic H2 Release from Precambrian Fractured Rocks—Energy for Deep Subsurface Life on Earth and Mars. Astrobiology, 7(6), 971–986. https://doi.org/10.1089/ast.2006.0096

Lusty, P. A., Lacinska, A. M., Millar, I. L., Barrie, C. D., & Boyce, A. J. (2017b). Volcanological and environmental controls on the Snowdon mineralization, North Wales, UK: A failed volcanogenic massive sulfide system in the Avalon Zone of the British Caledonides. Ore Geology Reviews, 89, 557–586. https://doi.org/10.1016/j.oregeorev.2017.06.031

Lévy, D., Boka-Mene, M., Meshi, A., Fejza, I., Guermont, T., Hauville, B., & Pelissier, N. (2023). Looking for natural hydrogen in Albania and Kosova. Frontiers in Earth Science, 11. https://doi.org/10.3389/feart.2023.1167634

Lévy, D., Roche, V., Pasquet, G., Combaudon, V., Geymond, U., Loiseau, K., & Moretti, I. (2023). Natural H2 exploration: tools and workflows to characterize a play. Science and Technology for Energy Transition, 78, 27. https://doi.org/10.2516/stet/2023021

Maier, W. D., Peltonen, P., Halkoaho, T., & Hanski, E. (2013). Geochemistry of komatiites from the Tipasjärvi, Kuhmo, Suomussalmi, Ilomantsi and Tulppio greenstone belts, Finland: Implications for tectonic setting and Ni sulphide prospectivity. Precambrian Research, 228, 63–84. https://doi.org/10.1016/j.precamres.2012.12.004

Maiga, O., Deville, E., Laval, J., Prinzhofer, A., & Diallo, A. B. (2023). Characterization of the spontaneously recharging natural hydrogen reservoirs of Bourakebougou in Mali. Scientific Reports, 13(1). https://doi.org/10.1038/s41598-023-38977-y

Marescotti, P., Comodi, P., Crispini, L., Gigli, L., Zucchini, A., & Fornasaro, S. (2019). Potentially Toxic Elements in Ultramafic Soils: A Study from Metamorphic Ophiolites of the Voltri Massif (Western Alps, Italy). Minerals, 9(8), 502. https://doi.org/10.3390/min9080502

Marques, J. M., Neves, M. O., Miller, A. Z., Rocha, C., Vance, S., Christensen, L., Etiope, G., Carreira, P. M., & Suzuki, S. (2017). Water-rock Interaction Ascribed to Hyperalkaline Mineral Waters in the Cabeço de Vide Serpentinized Ultramafic Intrusive Massif (Central Portugal). Procedia Earth and Planetary Science, 17, 646–649. https://doi.org/10.1016/j.proeps.2016.12.173

Marshak, S., & Van Der Pluijm, B. A. (2020). Tectonics of the continental interior in the United States. In Elsevier eBooks (pp. 173–186). https://doi.org/10.1016/b978-0-08-102908-4.00139-9

Mart Zijp, Nelskamp, S., & Doornenbal, H. (2017, March 19). European Unconventional Oil and Gas Assessment (EUOGA): Resource estimation of shale gas and shale oil in Europe. https://www.researchgate.net/publication/320490073_European_Unconventional_Oil_and_Gas_Assessment_EUOGA_Resource_estimation_of_shale_gas_and_shale_oil_in_Europe

Matenco, L., Balázs, A., Nader, F. H., Haq, B. U., & Fodor, L. (2021). Advances in the understanding of multi-scale and coupled evolution of orogens, sedimentary basins and the underlying lithosphere. Global and Planetary Change, 208, 103689. https://doi.org/10.1016/j.gloplacha.2021.103689

Mathur, Y., Awosiji, V., Mukerji, T., Scheirer, A. H., & Peters, K. E. (2023). Soil geochemistry of hydrogen and other gases along the San Andreas fault. International Journal of Hydrogen Energy, 50, 411–419. https://doi.org/10.1016/j.ijhydene.2023.09.032

Małachowska, A., Łukasik, N., Mioduska, J., & Gębicki, J. (2022). Hydrogen Storage in Geological Formations—The potential of salt caverns. Energies, 15(14), 5038. https://doi.org/10.3390/en15145038

McConnell, B., Riggs, N., & Fritschle, T. (2020). Tectonic history across the Iapetus suture zone in Ireland. Geological Society London Special Publications, 503(1), 333–345. https://doi.org/10.1144/sp503-2019-233

Melcher, F., Meisel, T., Puhl, J., & Koller, F. (2002). Petrogenesis and geotectonic setting of ultramafic rocks in the Eastern Alps: constraints from geochemistry. Lithos, 65(1–2), 69–112. https://doi.org/10.1016/s0024-4937(02)00161-5

Meshi, A., Boudier, F., Nicolas, A., & Milushi, I. (2009). Structure and tectonics of lower crustal and upper mantle rocks in the Jurassic Mirdita ophiolites, Albania. International Geology Review, 52(2–3), 117–141. https://doi.org/10.1080/00206810902823982

Mikrut, J., Matusiak-Małek, M., Ceuleneer, G., Grégoire, M., & Onuzi, K. (2024). Melt-rock interaction as a factor controlling evolution of chromite and olivine in dunite - case study from the Kukes Massif (Mirdita ophiolite, Albania). Journal of Geosciences, 49–64. https://doi.org/10.3190/jgeosci.386

Minissale, A., Magro, G., Martinelli, G., Vaselli, O., & Tassi, G. (2000). Fluid geochemical transect in the Northern Apennines (central-northern Italy): fluid genesis and migration and tectonic implications. Tectonophysics, 319(3), 199–222. https://doi.org/10.1016/s0040-1951(00)00031-7

Miró, J., Manatschal, G., Cadenas, P., & Muñoz, J. A. (2021). Reactivation of a hyperextended rift system: The Basque–Cantabrian Pyrenees case. Basin Research, 33(6), 3077–3101. https://doi.org/10.1111/bre.12595

Moilanen, M., Hanski, E., Konnunaho, J., Yang, S., Törmänen, T., Li, C., & Zhou, L. (2018). Re-Os isotope geochemistry of komatiite-hosted Ni-Cu-PGE deposits in Finland. Ore Geology Reviews, 105, 102–122. https://doi.org/10.1016/j.oregeorev.2018.12.007

Mężyk, M., Malinowski, M., & Mazur, S. (2021). Structure of a diffuse suture between Fennoscandia and Sarmatia in SE Poland based on interpretation of regional reflection seismic profiles supported by unsupervised clustering. Precambrian Research, 358, 106176. https://doi.org/10.1016/j.precamres.2021.106176

Nance, R. D., Gutiérrez-Alonso, G., Keppie, J. D., Linnemann, U., Murphy, J. B., Quesada, C., Strachan, R. A., & Woodcock, N. H. (2009). Evolution of the Rheic Ocean. Gondwana Research, 17(2–3), 194–222. https://doi.org/10.1016/j.gr.2009.08.001

Nenakhov, V. M., Polevanov, V. P., Zhabin, A. V., Bondarenko, S. V., & Zolotareva, G. S. (2023). Prospects for the discovery of natural hydrogen in the Voronezh anteclise. Doklady Earth Sciences, 513(S2), S182–S192. https://doi.org/10.1134/s1028334x23603474

Parnell, J., & Blamey, N. (2017). Global hydrogen reservoirs in basement and basins. Geochemical Transactions, 18(1). https://doi.org/10.1186/s12932-017-0041-4

Passaro, S., Tamburrino, S., Vallefuoco, M., Tassi, F., Vaselli, O., Giannini, L., Chiodini, G., Caliro, S., Sacchi, M., Rizzo, A. L., & Ventura, G. (2016). Seafloor doming driven by degassing processes unveils sprouting volcanism in coastal areas. Scientific Reports, 6(1). https://doi.org/10.1038/srep22448

Pawlewicz, M. J., Williams, A. J., Walden, S. M., Steinshouer, D. W., & Gautier, D. (2003). Geology of Europe including Turkey [Data set]. U.S. Geological Survey, Central Energy Resources Team. https://doi.org/10.5066/P9C8ZY5Q

Peltonen, P., & Kontinen, A. (2004b). The Jormua Ophiolite: a Mafic-Ultramafic Complex from an Ancient Ocean-Continent Transition Zone. In Developments in precambrian geology (pp. 35–71). https://doi.org/10.1016/s0166-2635(04)13001-6

Petrović, D., Cvetkov, V., Vasiljević, I., & Cvetković, V. (2015). A new geophysical model of the Serbian part of the East Vardar ophiolite: Implications for its geodynamic evolution. Journal of Geodynamics, 90, 1–13. https://doi.org/10.1016/j.jog.2015.07.003

Pin, C., Fonseca, P. E., Paquette, J., Castro, P., & Matte, P. (2008). The ca. 350 Ma Beja Igneous Complex: A record of transcurrent slab break-off in the Southern Iberia Variscan Belt? Tectonophysics, 461(1–4), 356–377. https://doi.org/10.1016/j.tecto.2008.06.001

Pin, C., Paquette, J. L., Ábalos, B., Santos, F. J., & Ibarguchi, J. I. G. (2006). Composite origin of an early Variscan transported suture: Ophiolitic units of the Morais Nappe Complex (north Portugal). Tectonics, 25(5). https://doi.org/10.1029/2006tc001971

Pitkänen, P., Ahokas, H., Ylä-Mella, M., Partamies, S., Snellman, M., & Hellä, P. (2007). Quality Review of Hydrochemical Baseline Data from the Olkiluoto Site. Posiva. Posiva Report No. 2007-5

Plissart, G., Monnier, C., Diot, H., Mărunţiu, M., Berger, J., & Triantafyllou, A. (2017). Petrology, geochemistry and Sm-Nd analyses on the Balkan-Carpathian Ophiolite (BCO – Romania, Serbia, Bulgaria): Remnants of a Devonian back-arc basin in the easternmost part of the Variscan domain. Journal of Geodynamics, 105, 27–50. https://doi.org/10.1016/j.jog.2017.01.001

Pomonis, P., & Magganas, A. (2017). Petrogenetic Implications for Ophiolite Ultramafic Bodies from Lokris and Beotia (Central Greece) Based on Chemistry of Their Cr-spinels. Geosciences, 7(1), 10. https://doi.org/10.3390/geosciences7010010

Prevorcic, R. (2014). Die Geologie des Kraubather Ultramafitkomplexes zwischen Wintergraben und Lobminggraben (Steiermark, Österreich). Leoben University. https://pure.unileoben.ac.at/portal/files/4425234/AC12181454n01.pdf

Prinzhofer, A., Moretti, I., Françolin, J., Pacheco, C., D'Agostino, A., Werly, J., & Rupin, F. (2019). Natural hydrogen continuous emission from sedimentary basins: The example of a Brazilian H2-emitting structure. International Journal of Hydrogen Energy, 44(12), 5676–5685. https://doi.org/10.1016/j.ijhydene.2019.01.119

Puga, E., De Federico, A. D., Fanning, M., Nieto, J., Martínez-Conde, J. R., Puga, M. D., Lozano, J., Bianchini, G., Natali, C., & Beccaluva, L. (2017). The Betic ophiolites and the mesozoic evolution of the Western Tethys. Geosciences, 7(2), 31. https://doi.org/10.3390/geosciences7020031

Putiš, M., Nemec, O., Ustalić, S., Babajić, E., Ružička, P., Koller, F., Kurylo, S., & Katanić, P. (2022). Mineralogical-Petrographical Record of Melt-Rock Interaction and P–T Estimates from the Ozren Massif Ophiolites (Bosnia and Herzegovina). Minerals, 12(9), 1108. https://doi.org/10.3390/min12091108

Pál-Molnár, E., Batki, A., Almási, E., Kiss, B., Upton, B. G., Markl, G., Odling, N., & Harangi, S. (2015). Origin of mafic and ultramafic cumulates from the Ditrău Alkaline Massif, Romania. Lithos, 239, 1–18. https://doi.org/10.1016/j.lithos.2015.09.022

Randazzo, P., Caracausi, A., Aiuppa, A., Cardellini, C., Chiodini, G., D'Alessandro, W., Vigni, L. L., Papic, P., Marinkovic, G., & Ionescu, A. (2021). Active degassing of deeply sourced fluids in central Europe: new evidences from a geochemical study in Serbia. Geochemistry Geophysics Geosystems, 22(11). https://doi.org/10.1029/2021gc010017

Rattey, R. P., & Hayward, A. B. (1993). Sequence stratigraphy of a failed rift system: the Middle Jurassic to Early Cretaceous basin evolution of the Central and Northern North Sea. Geological Society London Petroleum Geology Conference Series, 4(1), 215–249. https://doi.org/10.1144/0040215

Ring, U., & Pantazides, H. (2019). The uplift of the Troodos Massif, Cyprus. Tectonics, 38(8), 3124–3139. https://doi.org/10.1029/2019tc005514

Rizzo, A. L., Barberi, F., Carapezza, M. L., Di Piazza, A., Francalanci, L., Sortino, F., & D'Alessandro, W. (2015). New mafic magma refilling a quiescent volcano: Evidence from He-Ne-Ar isotopes during the 2011-2012 unrest at Santorini, Greece. Geochemistry Geophysics Geosystems, 16(3), 798–814. https://doi.org/10.1002/2014gc005653

Roberts, D., Nilsson, L. P., & Ramsay, D. M. (2005). The Raudfjellet ophiolite fragment, Central Norwegian Caledonides: principal lithological and structural features. https://hdl.handle.net/11250/2674161

Rohrman, M., Van Der Beek, P., & Andriessen, P. (1994). Syn-rift thermal structure and post-rift evolution of the Oslo Rift (southeast Norway): New constraints from fission track thermochronology. Earth and Planetary Science Letters, 127(1–4), 39–54. https://doi.org/10.1016/0012-821x(94)90196-1

Rosberg, J., & Erlström, M. (2021). Evaluation of deep geothermal exploration drillings in the crystalline basement of the Fennoscandian Shield Border Zone in south Sweden. Geothermal Energy, 9(1). https://doi.org/10.1186/s40517-021-00203-1

Roux, V. L., Bodinier, J., Tommasi, A., Alard, O., Dautria, J., Vauchez, A., & Riches, A. (2007). The Lherz spinel lherzolite: Refertilized rather than pristine mantle. Earth and Planetary Science Letters, 259(3–4), 599–612. https://doi.org/10.1016/j.epsl.2007.05.026

Saccani, E., Nicolae, I., & Tassinari, R. (2001). TECTONO-MAGMATIC SETTING OF THE JURASSIC OPHIOLITES FROM THE SOUTH APUSENI MOUNTAINS (ROMANIA): PETROLOGICAL AND GEOCHEMICAL EVIDENCE. Ofioliti, 26(1), 9–22. https://doi.org/10.4454/ofioliti.v26i1.127

Sano, S. (2002). Petrological, geochemical and isotopic constraints on the origin of the Harzburg intrusion, Germany. Journal of Petrology, 43(8), 1529–1549. https://doi.org/10.1093/petrology/43.8.1529

Saspiturry, N., Allanic, C., & Peyrefitte, A. (2024). Serpentinization and magmatic distribution in a hyperextended rift suture: Implication for natural hydrogen exploration (Mauléon Basin, Pyrenees). Tectonics, 43(8). https://doi.org/10.1029/2024tc008385

Schaltegger, U., Abrecht, J., & Corfu, F. (2003). The Ordovician orogeny in the Alpine basement: constraints from geochronology and geochemistry in the Aar Massif (Central Alps). Schweizerische Mineralogische Und Petrographische Mitteilungen, 83, 183–195. https://archive-ouverte.unige.ch/unige:28437

Schovsbo, N. H., Doornenbal, H., Nelskamp, S., Pedersen, C. B., Tougaard, L., Zijp, M., & Anthonsen, K. L. (2017). Review of results and recommendations. Delivery T8 of the EUOGA study (EU Unconventional Oil and Gas Assessment) commissioned by JRC-IET. European Commission. https://doi.org/10.22008/FK2/4JS6NW/6RLA3Z

Segvic, B. (2010). Petrologic and geochemical characteristics of the Krivaja-Konjuh ophiolite complex (NE Bosnia and Herzegovina) - petrogenesis and regional geodynamic implications. https://doi.org/10.11588/heidok.00010432

Slagstad, T., Pin, C., Roberts, D., Kirkland, C. L., Grenne, T., Dunning, G., Sauer, S., & Andersen, T. (2013). Tectonomagmatic evolution of the Early Ordovician suprasubduction-zone ophiolites of the Trondheim Region, Mid-Norwegian Caledonides. Geological Society London Special Publications, 390(1), 541–561. https://doi.org/10.1144/sp390.11

Smit, J., Van Wees, J., & Cloetingh, S. (2016). The Thor suture zone: From subduction to intraplate basin setting. Geology, 44(9), 707–710. https://doi.org/10.1130/g37958.1

Smith, N. J. P., Shepherd, T. J., Styles, M. T., & Williams, G. M. (2005). Hydrogen exploration: a review of global hydrogen accumulations and implications for prospective areas in NW Europe. Geological Society London Petroleum Geology Conference Series, 6(1), 349–358. https://doi.org/10.1144/0060349

Sreckovic-Batocanin, D., Vaskovic, N., Matovic, V., & Gajic, V. (2012). Correlation of metabasic rocks from metamorphic soles of the Dinaridic and the Western Vardar zone ophiolites (Serbia): Three contrasting pressure-temperature-time paths. Geoloski Anali Balkanskog Poluostrva, 73, 61–85. https://doi.org/10.2298/gabp1273061s

Stober, I., Teiber, H., Li, X., Jendryszczyk, N., & Bucher, K. (2017). Chemical composition of surface- and groundwater in fast-weathering silicate rocks in the Seiland Igneous Province, North Norway. Norwegian Journal of Geology. https://doi.org/10.17850/njg97-1-04

Suberu, M. Y., Mustafa, M. W., & Bashir, N. (2014). Energy storage systems for renewable energy power sector integration and mitigation of intermittency. Renewable and Sustainable Energy Reviews, 35, 499–514. https://doi.org/10.1016/j.rser.2014.04.009

Séjourné, S., Comeau, F., Santos, M. L. M. D., Bordeleau, G., Claprood, M., Mouge, P., Mulliez, V., Malo, M., Giroux, B., Gloaguen, E., & Raymond, J. (2024). Potential for natural hydrogen in Quebec (Canada): a first review. Frontiers in Geochemistry, 2. https://doi.org/10.3389/fgeoc.2024.1351631

Templeton, A. S., Ellison, E. T., Kelemen, P. B., Leong, J., Boyd, E. S., Colman, D. R., & Matter, J. M. (2024). Low-temperature hydrogen production and consumption in partially-hydrated peridotites in Oman: implications for stimulated geological hydrogen production. Frontiers in Geochemistry, 2. https://doi.org/10.3389/fgeoc.2024.1366268

Tremblay, A., Meshi, A., Deschamps, T., Goulet, F., & Goulet, N. (2015). The Vardar zone as a suture for the Mirdita ophiolites, Albania: Constraints from the structural analysis of the Korabi-Pelagonia zone. Tectonics, 34(2), 352–375. https://doi.org/10.1002/2014tc003807

Truche, L., Donzé, F., Goskolli, E., Muceku, B., Loisy, C., Monnin, C., Dutoit, H., & Cerepi, A. (2024). A deep reservoir for hydrogen drives intense degassing in the Bulqizë ophiolite. Science, 383(6683), 618–621. https://doi.org/10.1126/science.adk9099

Tugend, J., Manatschal, G., Kusznir, N. J., Masini, E., Mohn, G., & Thinon, I. (2014). Formation and deformation of hyperextended rift systems: Insights from rift domain mapping in the Bay of Biscay-Pyrenees. Tectonics, 33(7), 1239–1276. https://doi.org/10.1002/2014tc003529

Uliasz-Misiak, B., Lewandowska-Śmierzchalska, J., Matuła, R., & Tarkowski, R. (2022). Prospects for the implementation of underground hydrogen storage in the EU. Energies, 15(24), 9535. https://doi.org/10.3390/en15249535

Ustalić, S., Nemec, O., Milovská, S., Putiš, M., Babajić, E., Kurylo, S., & Ružička, P. (2024). Amphibole group minerals in the Ozren Massif ophiolites of Bosnia and Herzegovina as petrogenetic indicators. Minerals, 14(3), 239. https://doi.org/10.3390/min14030239

Utley, J. (2025, March 3). Natural hydrogen – the treasure hidden underground | FAU Erlangen-Nürnberg. FAU Erlangen-Nürnberg. https://www.fau.eu/2024/11/news/natural-hydrogen-the-treasure-hidden-underground

Virtanen, V. J., Höytiä, H. M., Iacono-Marziano, G., Yang, S., Moilanen, M., & Törmänen, T. (2024). From the mantle source to the crustal sink: magmatic differentiation and sulfide saturation of the Paleoproterozoic komatiites of the Central Lapland Greenstone Belt, Finland. Contributions to Mineralogy and Petrology, 179(7). https://doi.org/10.1007/s00410-024-02154-9

Wang, L., Jin, Z., Chen, X., Su, Y., & Huang, X. (2023). The origin and occurrence of natural hydrogen. Energies, 16(5), 2400. https://doi.org/10.3390/en16052400

Wybraniec, S., Zhou, S., Thybo, H., Forsberg, R., Perchuc, E., Lee, M., Demianov, G. D., & Strakhov, V. N. (1998). New map compiled of Europe's gravity field. Eos, 79(37), 437–442. https://doi.org/10.1029/98eo00330

Wójcik, K. (2024). Wodór naturalny w Polsce. Przegląd Geologiczny, 72(10), 584–596. https://doi.org/10.7306/2024.37

Xiang, Y., Sun, X., Liu, D., Yan, L., Wang, B., & Gao, X. (2020). Spatial distribution of RN, CO_2, HG, and H_2 concentrations in soil gas across a thrust fault in Xinjiang, China. Frontiers in Earth Science, 8. https://doi.org/10.3389/feart.2020.554924

Xiong, F., Yang, J., Robinson, P. T., Dilek, Y., Milushi, I., Xu, X., Chen, Y., Zhou, W., Zhang, Z., Lai, S., Tian, Y., & Huang, Z. (2015). Petrology and geochemistry of high Cr# podiform chromitites of Bulqiza, Eastern Mirdita Ophiolite (EMO), Albania. Ore Geology Reviews, 70, 188–207. https://doi.org/10.1016/j.oregeorev.2015.04.011

Zgonnik, V. (2020). The occurrence and geoscience of natural hydrogen: A comprehensive review. Earth-Science Reviews, 203, 103140. https://doi.org/10.1016/j.earscirev.2020.103140

Zgonnik, V., Beaumont, V., Deville, E., Larin, N., Pillot, D., & Farrell, K. M. (2015). Evidence for natural molecular hydrogen seepage associated with Carolina bays (surficial, ovoid depressions on the Atlantic Coastal Plain, Province of the USA). Progress in Earth and Planetary Science, 2(1). https://doi.org/10.1186/s40645-015-0062-5

Zuo, J., Webb, A. a. G., Chin, E. J., Ackerman, L., Harvey, J., Haproff, P. J., Müller, T., Wang, Q., Hickman, A. H., Sorger, D., & Ramírez-Salazar, A. (2022). Earth's Earliest Phaneritic Ultramafic Rocks: Mantle Slices or Crustal Cumulates? Geochemistry Geophysics Geosystems, 23(12). https://doi.org/10.1029/2022gc010519

Zwaan, F., Brune, S., Glerum, A. C., Vasey, D. A., Naliboff, J. B., Manatschal, G., & Gaucher, E. C. (2025). Rift-inversion orogens are potential hot spots for natural H_2 generation. Science Advances, 11(8). https://doi.org/10.1126/sciadv.adr3418

Supplementary Material for

Mapping Europe's Natural Hydrogen Potential: A Continental-Scale Geological Prospectivity Assessment

This supplementary material contains:

1. Supplementary Tables
2. Supplementary Figures
3. Supplementary Methodology

A1. Supplementary Tables

Table A. 1 | *Compilation of surface ultramafic rocks and ophiolites with ultramafic character. The country of each body is listed, along with (if known) the depth of ultramafic rock, the degree of serpentinization, and the types of ultramafic rock. High favorability (+) is assigned if within 4-21 km, based on the temperature range of serpentinization and the varying geothermal gradient in Europe; low favorability (-) is assigned if outside this range. If unknown, no favorability is assigned (o).*

#	Name of ophiolite or ultramafic body	Country	Depth	Degree of serpentinization	Types of ultramafic rock	Favorability	Source
1	Seiland igneous province	Norway	9-17 km		Dunite, wehrlite	+	Pastore et al., 2016; Pastore et al., 2024
2	Leka ophiolite complex	Norway	4 km		Dunite, harzburgite, wehrlite, pyroxenite	+	Michels et al., 2020
3	Central Sudetic ophiolites	Poland, Czech Republic	4-12 km	Partial	Harzburgite, lherzolite, pyroxene-rich cumulates	+	Kryza & Pin, 2009
4	Mauleon Basin & Saint-Gaudens	France	10-17 km	35-39%	Peridotite	+	Chevrot et al., 2018; Lefeuvre et al., 2021; Pajang et al., 2025
5	Lherz peridotite massif	France	Shallow to mid-crustal		Peridotite	+	Asti et al., 2024
6	Careon ophiolite & Ordenes complex	Spain	>15 km	Partial	Harzburgite, dunite	+	Garcia et al., 1999
7	Vila de Cruces & Bazar ophiolitic units	Spain	3-5 km		Peridotite, dunite	+	Arenas et al., 2007; Moreno et al., 2001
8	Troodos ophiolite	Cyprus	2-8 km		Harzburgite, dunite, wehrlite, pyroxenite	+	Ring & Pantazides, 2019; George, 1978
9	Shetland ophiolite complex	Scotland	3-8 km	~100%	Serpentinite	+	Flinn, 2001
10	Ronda massif	Spain	5 km		Peridotite	+	
11	Balkan-Carpathian ophiolite	Romania, Serbia, Bulgaria	10 km	Partial	Harzburgite, dunite	+	Plissart et al., 2017

12	Tropoje massif	Albania, Kosovo	0-6 km		Harzburgite, dunite	+	Beqiraj et al., 2000
13	Kukes massif	Albania	0-7 km		Harzburgite, dunite, pyroxenite	+	Mikrut et al., 2024
14	Bulqize massif (Eastern Mirdita ophiolite)	Albania	0-6 km	Partial	Harzburgite, dunite	+	Beqiraj et al., 2000; Xiong et al., 2015
15	Eastern Rhodope region	Greece	> 2 km	Partial	Peridotite, dunite	o	Maltezou & Loucoyannakis, 1993
16	Raudfjellet ophiolite	Norway	500 m, suggested to extend deeper		Dunite, harzburgite, websterite	o	Roberts et al., 2005; Slagstad et al., 2013
17	Lapland greenstone belt	Finland			Komatiite	o	Heggie et al., 2013; Virtanen et al., 2024
18	Jormua ophiolite	Finland		Partial	Peridotite	o	Peltonen & Kontinen, 2004
19	Kuhmo & Suomussalmi greenstone belts	Finland		Partial	Komatiite, olivine-pyroxene cumulates	o	Konnunaho et al., 2015; Maier et al., 2013
20	Harz mountains	Germany	350 m, extend deeper	Partial	Dunite, harzburgite	o	Sano, 2002
21	Kraubath massif	Austria			Dunite, peridotites, pyroxenite	o	Prevorcic, 2014
22	Reckner complex & Matrei zone	Austria		Partial	Harzburgite, lherzolite, dunite	o	Melcher et al., 2002
23	Aar massif	Austria, Switzerland	Mid-crustal	~100%	Serpentinite	o	Schaltegger et al., 2003
24	Limousin ophiolite	France	1 km, suggested to extend deeper	Partial	Harzburgite, dunite, wehrlite	o	Berger et al., 2005
25	Champtoceaux ophiolite	France		Partial	Peridotite, dunite	o	Aertgeerts, 2016
26	Morais Nappe complex	Portugal			Harzburgite, dunite	o	Pin et al., 2006
27	Beja complex	Portugal			Peridotite, pyroxenite	o	Pin et al., 2008; Jesus et al., 2007
28	Pohorje mountains massif	Slovenia	1.5 km, suggested to extend deeper	Partial	Harzburgite, lherzolite, dunite	o	De Hoog et al., 2008
29	Rocchetta Vara ophiolite	Italy			Harzburgite, lherzolite, dunite	o	Sanfilipo et al., 2014; Schwarzenbach et al., 2021
30	Val Graveglia unit	Italy			Peridotite	o	Donzé et al., 2024
31	Bracco unit	Italy		Partial	Peridotite	o	

32	Balmuccia peridotite body, Piedmont-Ligurian ophiolite	Italy	4 km, suggested to extend deeper	< 5%	Peridotite	o	Ryberg et al., 2023
33	Voltri massif	Italy		Partial	Peridotite	o	Marescotti et al., 2019
34	Elba island ophiolite	Italy		Partial	Harzburgite, lherzolite, dunite	o	Frassi et al., 2017
35	Lesvos island, Samothraki island, Evros, Crete	Greece			Harzburgite, dunite	o	Koglin, 2008; Koglin et al., 2008
36	Brezovica ultramafic massif, Central Dinaridde Belt	Serbia	0.5 km, suggested to extend deeper		Harzburgite, dunite	o	Sreckovic-Batocanin et al., 2022; Bazylev et al., 2003
37	East Vardar ophiolite, Zdraljica and Kursumlija massifs	Serbia	2-3 km, suggested to extend deeper		Harzburgite, lherzolite	o	Petrovic et al., 2015
38	Krivaja-Konjuh complex	Bosnia & Herzegovina	0-2 km, suggested to extend deeper	Partial	Lherzolite, dunite, pyroxenite	o	Balen & Massonne, 2021; Segvic et al., 2010
39	Goleshi massif, Vardar zone	Kosovo	Surface, could extend deeper	Partial	Harzburgite, dunite	o	Fejza et al., 2010
40	Drenas region	Kosovo		Partial	Harzburgite	o	Fejza et al., 2022
41	Puka massif, Krabbi massif (Western Mirdita ophiolite)	Albania	0-3 km		Harzburgite, lherzolite	o	Mikrut et al., 2024; Meshi et al., 2009; Bogatu et al., 2019
42	Rommaneo complex	Finland	3 km		Komatiite, peridotite, dunite, pyroxenite	-	Moilanen et al., 2018
43	Kovero complex	Finland	3 km		Komatiite, peridodite, dunite, pyroxenite	-	Moilanen et al., 2018
44	Beaunit xenoliths	France	30 km		Dunite, lherzolite, harzburgite, websterite	-	Féménias et al., 2003
45	Betic Cordillera system	Spain	1-1.5 km	Partial	Peridotite (lherzolite)	-	Puga et al., 2011; Puga et al., 1999
46	East Othris ophiolite	Greece	Mantle depth	Partial	Harzburgite, lherzolite	-	Magganas & Koutsovitis, 2015
47	Northeast Pelopennesus	Greece	< 2 km		Peridotite	-	Tzanis et al., 2017
48	Ozren complex	Bosnia & Herzegovina	0 km		Harzburgite, lherzolite,	-	Putiš et al., 2022;

		dunite, troctolite	Ustalić et al., 2024

Table A. 2 | *Sources used for the different sublayers: serpentinization (SER), radiolysis (RAD), deep source (DEE), reservoir (RES), and seal (SEA). Sources contain either geological datasets of which parts were used, or contain maps which were georeferenced.*

Layer		**Sources**
SER1	Ultramafic rocks (-)	See table A.1 in appendix
SER2	Ultramafic rocks (o)	See table A.1 in appendix
SER3	Ultramafic rocks (+)	See table A.1 in appendix
SER4	Failed rifts	Tugend et al., 2014; Miro et al., 2021; Campbell et al., 1988; Lusty et al., 2017; Havlicek et al., 2024; Dèzes et al., 2004; Kübler et al., 2016; Fraefel, 2008; Cloetingh & Cornu, 2005; Rohrman et al., 1994.
SER5	Gravity anomalies	Bureau Gravimetrique International, 2012
SER6	Banded iron formations	Asch, 2005
SER7	Rift-inversion orogens	Zwaan et al., 2025
RAD1	Uranium occurrence	EGDI - INSPIRE, 2021
RAD2	Precambrian craton	Gee & Stephenson, 2006; Mezyk et al., 2021
RAD3	Accreted terranes	Inverse of layer RAD2
DEE1	Faults	Asch, 2005
DEE2	Suture zones	Pharaoh, 1990; McConnell et al., 2020; Nance et al., 2009; Smit et al., 2016; Khogenkumar et al., 2015; Tremblay et al., 2015; Matenco et al., 2021; Handy et al., 2019; Zelic et al., 2010
DEE3	High heat flow	Chamorro et al., 2013
DEE4	High heat flow buffer	Chamorro et al., 2013
RES1 / SEA2	Sedimentary rocks	Asch, 2005
RES2 / SEA3	Igneous and metamorphic rocks	Inverse of layer RES1 / SEA2
RES3 / SEA4	Sedimentary basins	Schovsbo et al., 2017; EUOGA, 2017.
SEA1	Subsurface salt	Kumar et al., 2021; Blanco & Faaij, 2017; Bermejo et al., 2017 ; Malachowska et al., 2022

B. Supplementary Figures

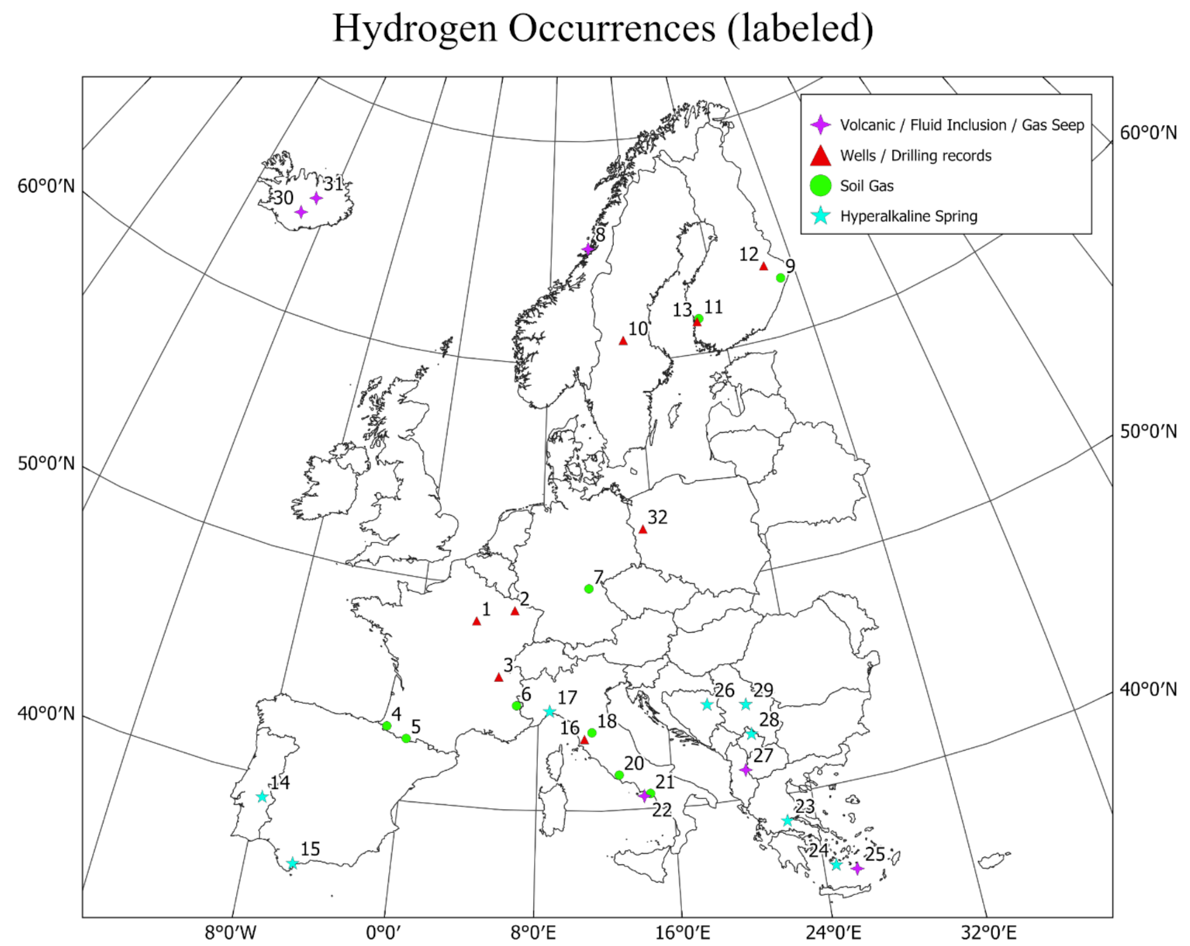

Figure B. 1 | *Map of hydrogen occurrences in Europe. Different colors/shapes represent different types of measurements. Labels correspond to table A.3, appendix.*

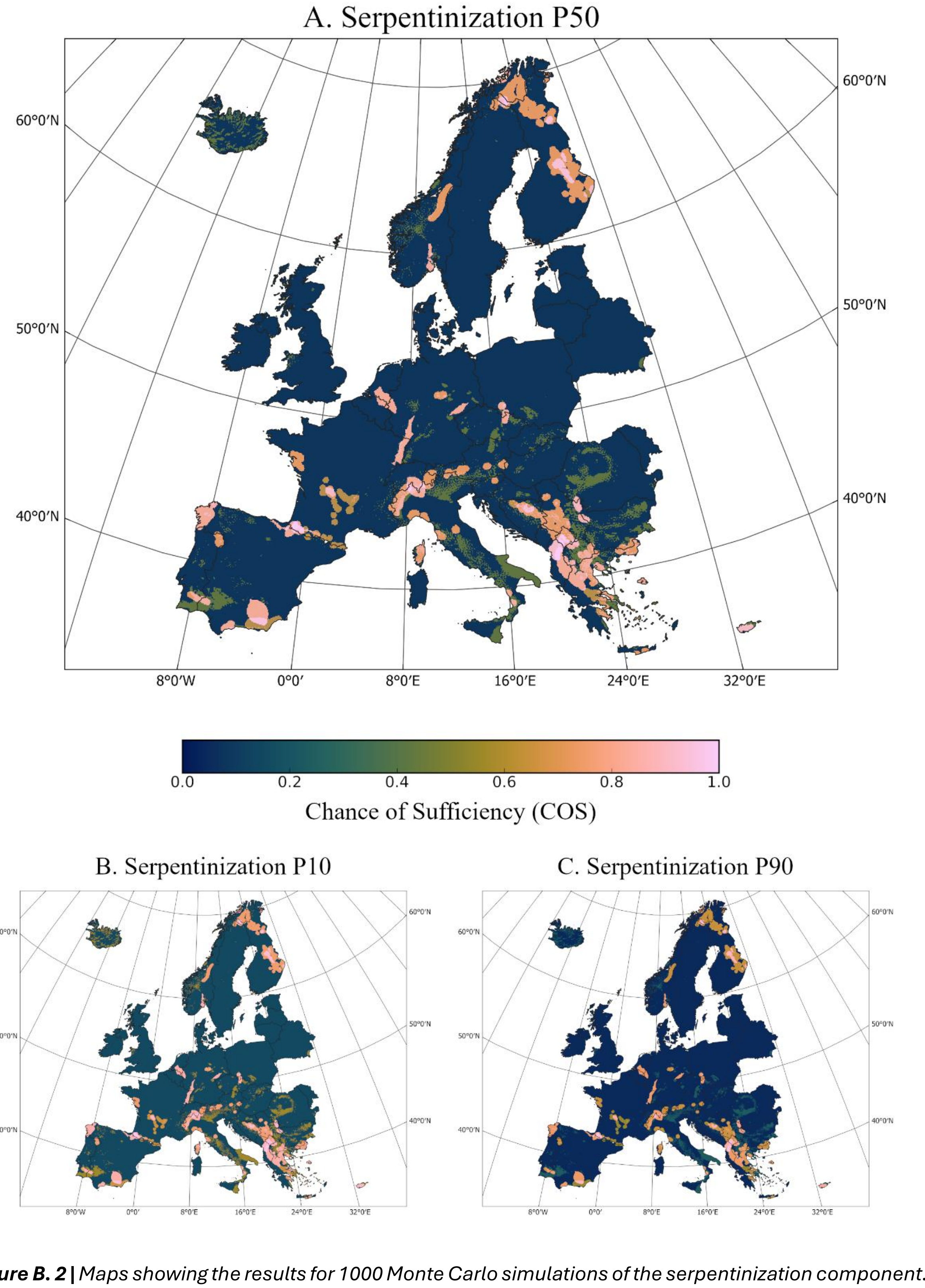

Figure B. 2 | *Maps showing the results for 1000 Monte Carlo simulations of the serpentinization component.* ***A,*** *median, 50 percent of runs exceed this COS value;* ***B*** *and* ***C,*** *10 percent and 90 percent of runs exceed this value, respectively.*

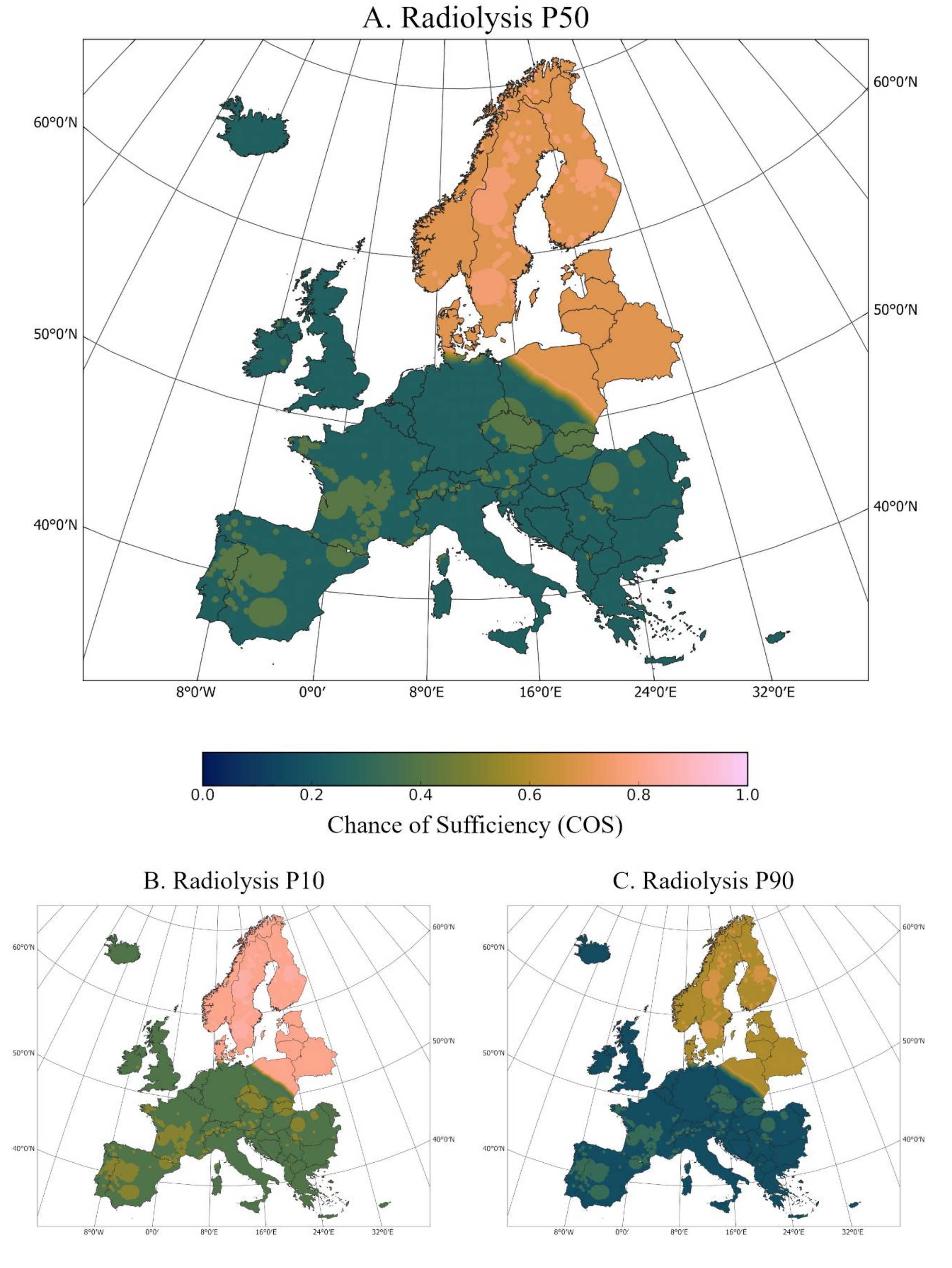

Figure B. 3 | *Maps showing the results for 1000 Monte Carlo simulations of the radiolysis component.* ***A,*** *median, 50 percent of runs exceed this COS value;* ***B*** *and* ***C,*** *10 percent and 90 percent of runs exceed this value, respectively.*

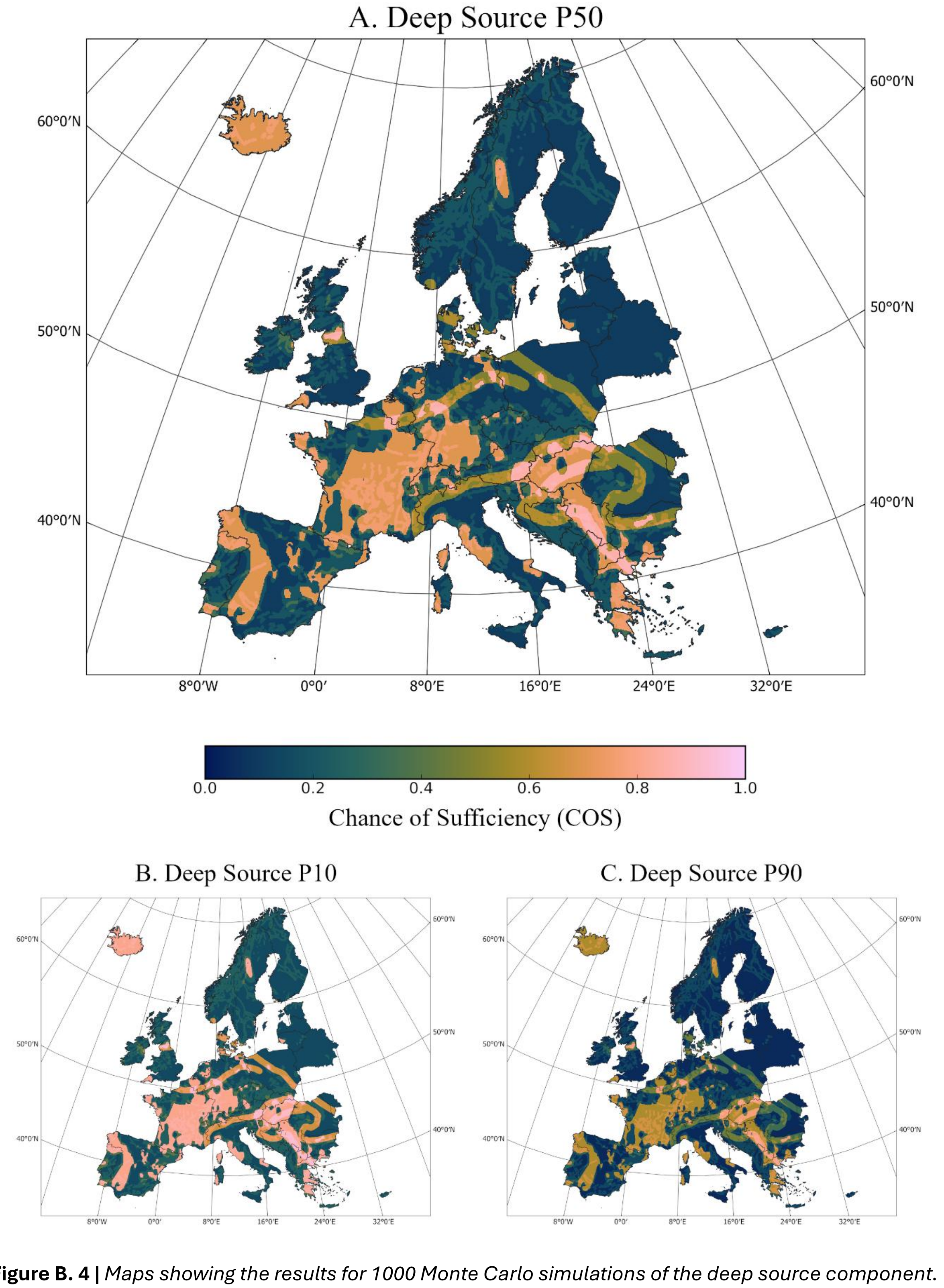

Figure B. 4 | *Maps showing the results for 1000 Monte Carlo simulations of the deep source component.* ***A,*** *median, 50 percent of runs exceed this COS value;* ***B*** *and* ***C****, 10 percent and 90 percent of runs exceed this value, respectively.*

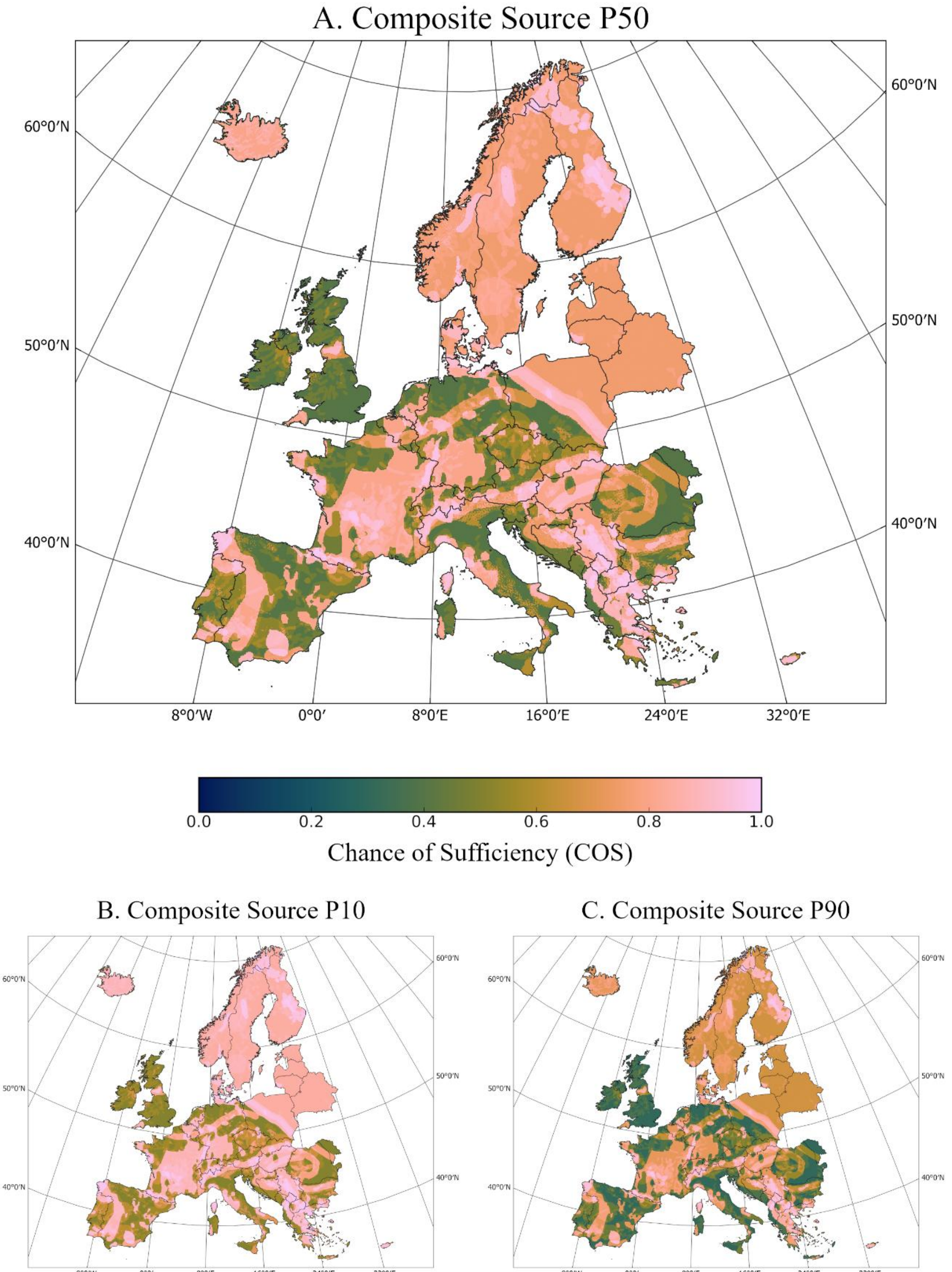

Figure B. 5 | *Maps showing the results for 1000 Monte Carlo simulations of the composite source component.* ***A,*** *median, 50 percent of runs exceed this COS value;* ***B*** *and* ***C****, 10 percent and 90 percent of runs exceed this value, respectively.*

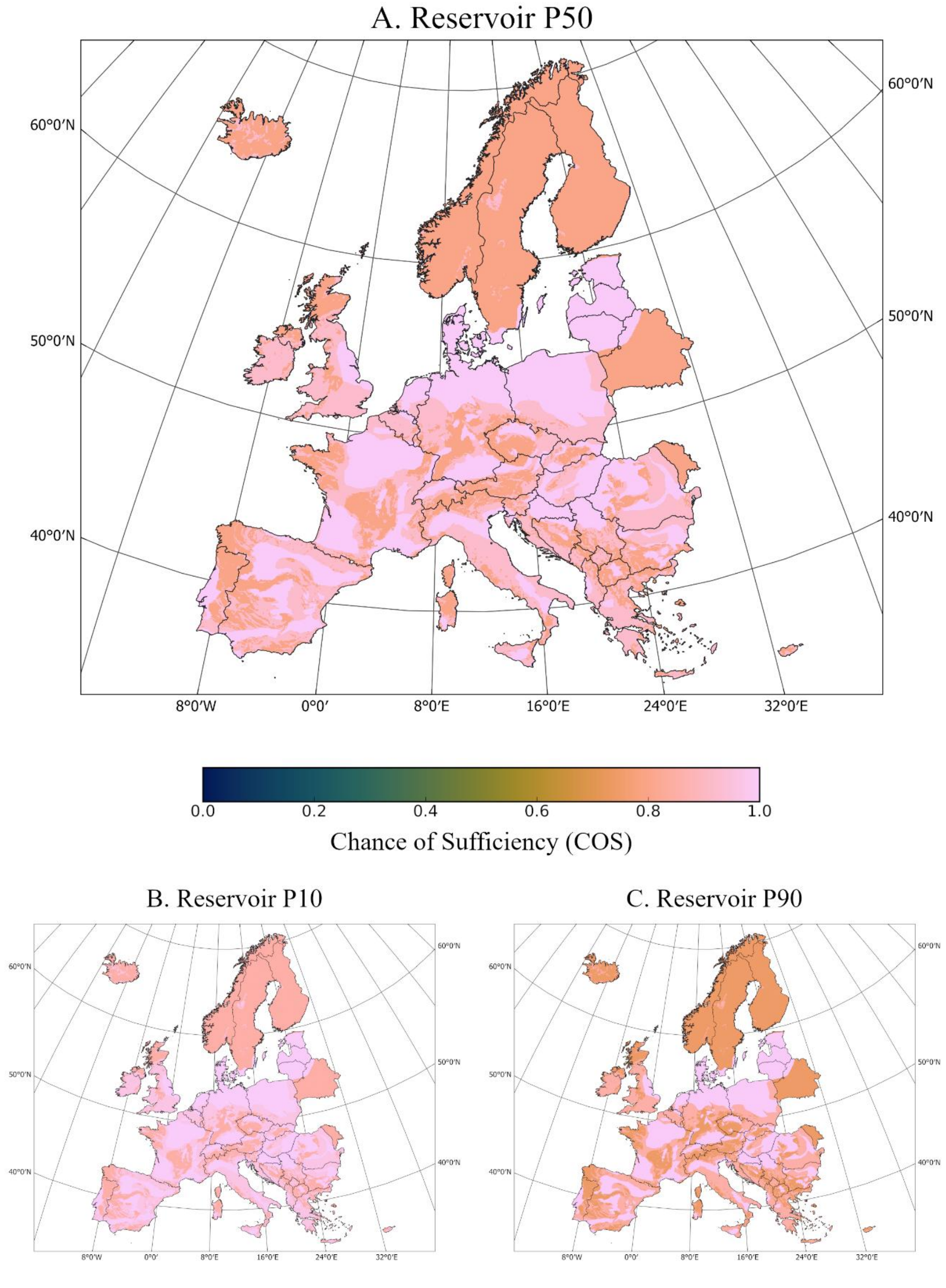

Figure B. 6 | *Maps showing the results for 1000 Monte Carlo simulations of the reservoir component.* ***A,*** *median, 50 percent of runs exceed this COS value;* ***B*** *and* ***C,*** *10 percent and 90 percent of runs exceed this value, respectively.*

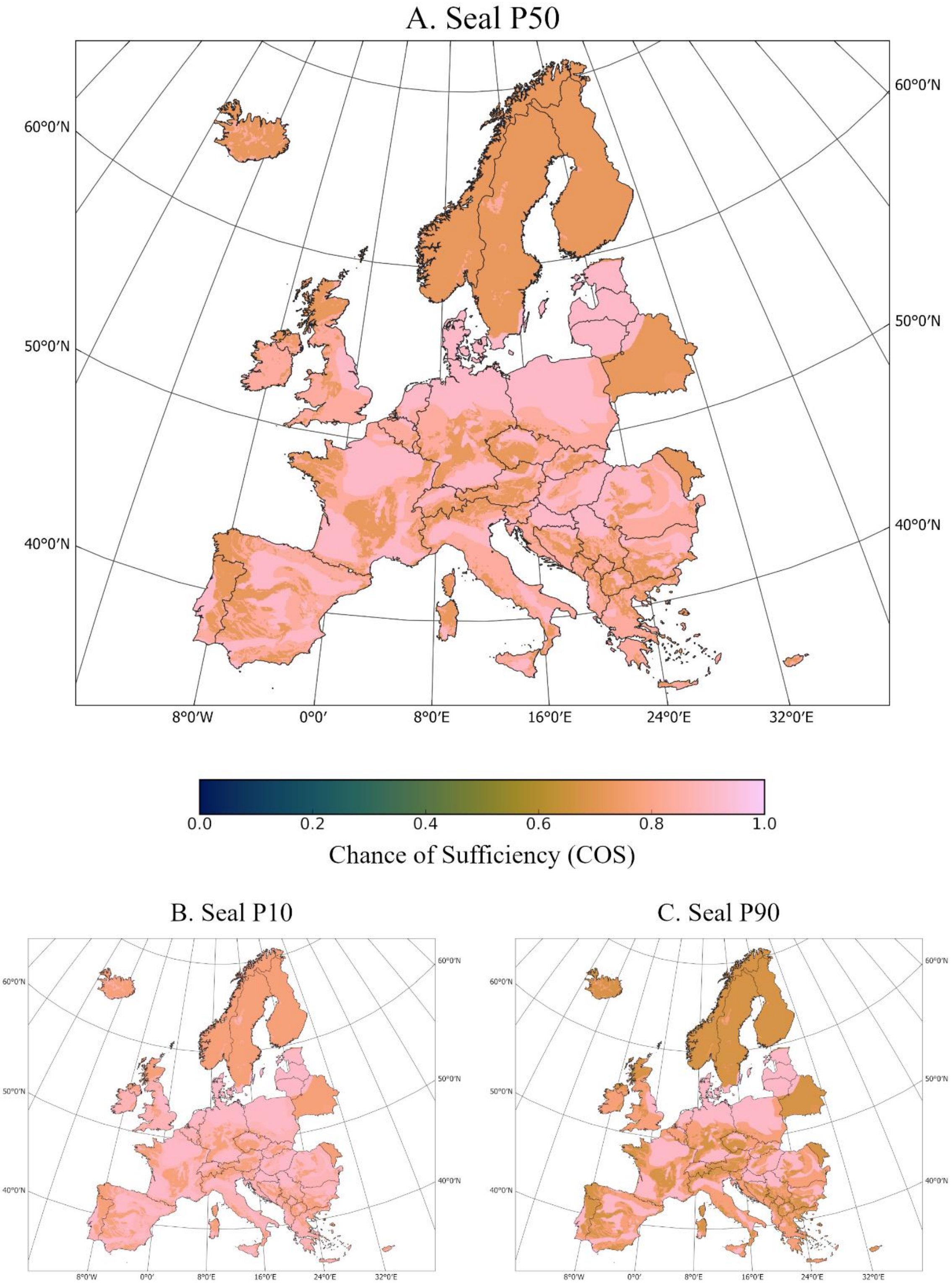

Figure B. 7 | *Maps showing the results for 1000 Monte Carlo simulations of the seal component.* ***A,*** *median, 50 percent of runs exceed this COS value;* ***B*** *and* ***C****, 10 percent and 90 percent of runs exceed this value, respectively.*

C. Supplementary methodology

C.1 Uranium Occurrence Buffer

The dataset of uranium occurrences represent different sizes of uranium deposits, as explained by the INSPIRE guidelines document (INSPIRE, 2024). Based on these sizes, the buffer is calculated using the equation:

$$r = R \cdot \sqrt{\frac{T}{T0}}$$

Where r = buffer, R is the buffer radius assigned to median tonnage T0 (the buffer for small deposits is set at 20 km), and T is he tonnage of the deposit size to be calculated. Resulting buffers are found in table C.1 below. This calculation is based on and accounts for the assumption that the mass of uranium in a deposit scales with its footprint area. This is used because no data exists on the subsurface extent of uranium in Europe.

Table C. 1 | *Buffer size assigned to different uranium deposits, based on the calculation above, and the deposit size as determined by INSPIRE.*

	Very large	**Large**	**Medium**	**Small**	**Unit**
Median Deposit Size	100000	60000	12500	2750	t (1 000 kg)
Buffer radius	120.6	93.4	42.6	20	km

C.2 Calculations for Composite Maps

The calculation of each component largely follows that used by Gelman et al. (2025), adapted to fit the indicators used here. Hydrogen prospectivity is described by:

$$P = COS_{SOURCE} \cdot COS_{RESERVOIR} \cdot COS_{SEAL}$$

Where P is the value determining hydrogen prospectivity, and COS is the chance of sufficiency associated with the 3 components. The COS values of all composite layers are calculated as:

$$COS_x = 1 - \prod_i (1 - COS_i)$$

Where *x* is the name of the component (e.g. serpentinization, composite source) and *i* describes the sublayers it contains. This method is used as opposed to using COS directly, because it determines that sublayers stack diminishingly; not every type of source needs to be present for a high prospectivity score.

C.3 Code Monte Carlo Simulation

The code used for the triangular distribution Monte Carlo simulation can be found below. The majority of code is reused for each layer.

Sublayers:

```
!pip install rasterio
import numpy as np
import rasterio
from rasterio.plot import show
from rasterio.transform import from_origin
from rasterio.enums import Resampling
import os
from tqdm import tqdm

# layer file names
layer_files = {
    'ultramafics_low': 'ULTRAMAFICS LOW FINAL.tif',
    'ultramafics_med': 'ULTRAMAFICS MED FINAL.tif',
    'ultramafics_high': 'ULTRAMAFICS HIGH FINAL.tif',
    'gravity_40': 'GRAVITY FINAL 2.tif',
    'failed_rifts': 'FAILED RIFTS FINAL.tif',
    'rift_inversion_orogens': 'RIFT INVERSION OROGENS FINAL.tif',
    'banded_iron_formations': 'BANDED IRON FORMATIONS FINAL 2.tif',
    'new_fallback_serpentinization': 'SERPENTINIZATION FALLBACK FINAL 2.tif',
    'uranium': 'URANIUM FINAL.tif',
    'precambrian_craton': 'PRECAMBRIAN CRATON FINAL 2.tif',
    'accreted_terranes': 'ACCRETED TERRANES FINAL.tif',
    'faults': 'FAULTS FINAL.tif',
    'sutures': 'SUTURES FINAL.tif',
    'heatflow_80': 'HEATFLOW FINAL.tif',
    'heatflow_7080': 'HEATFLOW BUFFER FINAL.tif',
    'fallback_for_deepsource': 'FALLBACK DEEPSOURCE FINAL.tif',
    'sedimentary_rocks': 'SEDIMENTARY ROCKS FINAL.tif',
    'crystalline_rocks': 'CRYSTALLINE ROCKS FINAL.tif',
    'sedimentary_basins': 'SEDIMENTARY BASINS FINAL.tif',
    'salt': 'SALT FINAL.tif'
}

cos_values = {
    'ultramafics_low': (0.5, 0.6, 0.7),
    'ultramafics_med': (0.6, 0.7, 0.8),
    'ultramafics_high': (0.7, 0.8, 0.9),
    'gravity_40': (0.1, 0.4, 0.7),
    'failed_rifts': (0.7, 0.8, 0.9),
    'rift_inversion_orogens': (0.7, 0.8, 0.9),
    'banded_iron_formations': (0.6, 0.7, 0.8),
    'new_fallback_serpentinization': (0.0, 0.1, 0.2),
```

```python
    'uranium': (0.1, 0.2, 0.3),
    'precambrian_craton': (0.5, 0.7, 0.9),
    'accreted_terranes': (0.1, 0.2, 0.5),
    'faults': (0.1, 0.2, 0.3),
    'sutures': (0.2, 0.5, 0.8),
    'heatflow_80': (0.5, 0.7, 0.9),
    'heatflow_7080': (0.1, 0.2, 0.3),
    'fallback_for_deepsource': (0.0, 0.1, 0.2),
    'sedimentary_rocks': (0.8, 0.95, 1.0),
    'crystalline_rocks': (0.7, 0.8, 0.9),
    'sedimentary_basins': (0.9999, 1.0, 1.0001),
    'salt': (0.0, 0.1, 0.2)
}

n_simulations = 1000

# sampling function for triangular distribution
def sample_cos(layer, shape):
    low, mid, high = cos_values[layer]
    return np.random.triangular(low, mid, high, size=shape).astype(np.float32)

# Loading rasters (all rasters must be same size!)
def load_rasters():
    data = {}
    ref_shape = None
    ref_meta = None
    for key, path in layer_files.items():
        with rasterio.open(path) as src:
            arr = src.read(1, resampling=Resampling.nearest)
            if ref_shape is not None and arr.shape != ref_shape:
                raise ValueError(f"Raster size mismatch: {path} has shape {arr.shape}, expected
{ref_shape}")
            data[key] = (arr > 0).astype(np.uint8)
            if ref_shape is None:
                ref_shape = arr.shape
                ref_meta = src.meta
    return data, ref_shape, ref_meta

# definitions
def combine_layers(logic_layers, sampled_vals):
    result = 1.0
    for layer in logic_layers:
        result *= (1 - sampled_vals[layer] * logic_layers[layer])
    return 1 - result

def combine_group(groups):
    result = 1.0
    for group in groups:
```

```
        result *= (1 - group)
    return 1 - result

# Main simulation loop
def run_simulation():
    layers, shape, meta = load_rasters()
    meta.update(dtype='float32', count=1)

    stats = []
    batch_size = 100
    for batch_start in tqdm(range(0, n_simulations, batch_size)):
        batch_end = min(batch_start + batch_size, n_simulations)
        batch_results = []
```

```
        for _ in range(batch_start, batch_end):
            sampled = {k: sample_cos(k, shape) for k in layer_files.keys()}
            COS_RD = combine_layers({k: layers[k] for k in [
                'uranium', 'precambrian_craton', 'accreted_terranes']}, sampled)
            batch_results.append(COS_RD)

        stack = np.stack(batch_results)
        stats.append({
            'P10': np.percentile(stack, 10, axis=0),
            'P50': np.percentile(stack, 50, axis=0),
            'P90': np.percentile(stack, 90, axis=0)
        })

    for perc in ['P10', 'P50', 'P90']:
        final_stack = np.stack([b[perc] for b in stats])
        final_output = np.mean(final_stack, axis=0)
        with rasterio.open(f'RD_{perc}.tif', 'w', **meta) as dst:
            dst.write(final_output.astype('float32'), 1)

# Run
run_simulation()
```

The code shown above is for the radiolysis component. For the other components, the last section of code is adapted to match that component.

For the final prospectivity map, a different loop is used:

```
# Main simulation loop
def run_simulation():
    layers, shape, meta = load_rasters()
    meta.update(dtype='float32', count=1)

    stats = []
```

```python
    batch_size = 100
    for batch_start in tqdm(range(0, n_simulations, batch_size)):
        batch_end = min(batch_start + batch_size, n_simulations)
        batch_results = []

        for _ in range(batch_start, batch_end):
            sampled = {k: sample_cos(k, shape) for k in layer_files.keys()}
            COS_SP = combine_layers({k: layers[k] for k in [
                'ultramafics_low','ultramafics_med','ultramafics_high',
                'gravity_40','failed_rifts','rift_inversion_orogens',
                'banded_iron_formations','new_fallback_serpentinization']}, sampled)
            COS_RD = combine_layers({k: layers[k] for k in [
                'uranium', 'precambrian_craton', 'accreted_terranes']}, sampled)
            COS_DP = combine_layers({k: layers[k] for k in [
                'faults', 'sutures', 'heatflow_80', 'heatflow_7080', 'fallback_for_deepsource']}, sampled)
            COS_SC = combine_group([
                combine_layers({k: layers[k] for k in [
                    'ultramafics_low','ultramafics_med','ultramafics_high',
                    'gravity_40','failed_rifts','rift_inversion_orogens',
                    'banded_iron_formations','new_fallback_serpentinization']}, sampled),
                combine_layers({k: layers[k] for k in [
                    'uranium', 'precambrian_craton', 'accreted_terranes']}, sampled),
                combine_layers({k: layers[k] for k in [
                    'faults', 'sutures', 'heatflow_80', 'heatflow_7080', 'fallback_for_deepsource']}, sampled)
            ])
            COS_RS = combine_layers({k: layers[k] for k in [
                'sedimentary_rocks', 'crystalline_rocks', 'sedimentary_basins']}, sampled)
            COS_SL = combine_layers({k: layers[k] for k in [
                'salt', 'sedimentary_rocks', 'crystalline_rocks', 'sedimentary_basins']}, sampled)
            COS_Final = COS_SC * COS_RS * COS_SL
            batch_results.append(COS_Final)

        stack = np.stack(batch_results)
        stats.append({
            'P10': np.percentile(stack, 10, axis=0),
            'P50': np.percentile(stack, 50, axis=0),
            'P90': np.percentile(stack, 90, axis=0)
        })

    for perc in ['P10', 'P50', 'P90']:
        final_stack = np.stack([b[perc] for b in stats])
        final_output = np.mean(final_stack, axis=0)
        with rasterio.open(f'Final_{perc}.tif', 'w', **meta) as dst:
            dst.write(final_output.astype('float32'), 1)

# Run everything
run_simulation()
```